AD-A143 767 APPLICATION OF SURFACE MAGNETOPLASMONS ON SEMICONDUCTOR 1/2
SUBSTRATES(U) BROWN UNIV PROVIDENCE RI
D M BOLLE ET AL. 31 DEC 83 ARO-17344.1-EL
UNCLASSIFIED DAAG29-80-K-0074 F/G 20/12 NL

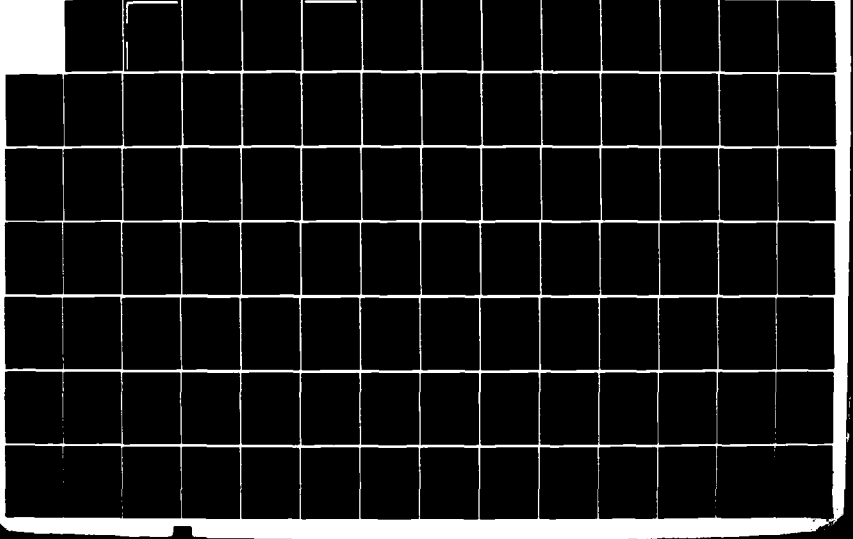

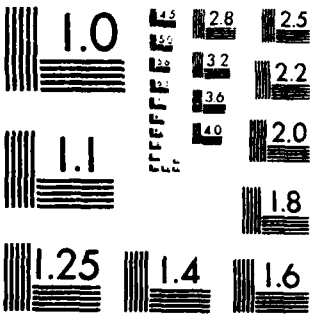

SECURITY CLASSIFICATION OF THIS PAGE *(When Data Entered)*

REPORT DOCUMENTATION PAGE

READ INSTRUCTIONS BEFORE COMPLETING FORM

1. REPORT NUMBER: ARO 17344.1-EL
2. GOVT ACCESSION NO.
3. RECIPIENT'S CATALOG NUMBER

4. TITLE *(and Subtitle)*: Application of Surface Magnetoplasmons on Semiconductor Substrates

5. TYPE OF REPORT & PERIOD COVERED: Final Report 9/22/80 - 12/31/83

6. PERFORMING ORG. REPORT NUMBER

7. AUTHOR(s): Donald M. Bolle, A. V. Nurmikko, and G.S. Heller

8. CONTRACT OR GRANT NUMBER(s): DAAG29-80-K-0074

9. PERFORMING ORGANIZATION NAME AND ADDRESS: Brown University, Providence, R.I. 02912, and Lehigh University, Bethlehem, PA 18015

10. PROGRAM ELEMENT, PROJECT, TASK AREA & WORK UNIT NUMBERS

11. CONTROLLING OFFICE NAME AND ADDRESS: U. S. Army Research Office, Post Office Box 12211, Research Triangle Park, NC 27709

12. REPORT DATE: 12/31/83

13. NUMBER OF PAGES

14. MONITORING AGENCY NAME & ADDRESS *(if different from Controlling Office)*

15. SECURITY CLASS. *(of this report)*: Unclassified

15a. DECLASSIFICATION/DOWNGRADING SCHEDULE

16. DISTRIBUTION STATEMENT *(of this Report)*

Approved for public release; distribution unlimited.

17. DISTRIBUTION STATEMENT *(of the abstract entered in Block 20, if different from Report)*

18. SUPPLEMENTARY NOTES

The view, opinions, and/or findings contained in this report are those of the author(s) and should not be construed as an official Department of the Army position, policy, or decision, unless so designated by other documentation

19. KEY WORDS *(Continue on reverse side if necessary and identify by block number)*

magnetoplasmons
substrates
sub-millimeter wavelength
millimeter wavelength

20. ABSTRACT *(Continue on reverse side if necessary and identify by block number)*

Attached

DD FORM 1 JAN 73 1473 EDITION OF 1 NOV 65 IS OBSOLETE

UNCLASSIFIED

Abstract

A significant need exists for developing active and passive components in the millimeter (MM) and submillimeter (SMM) wavelength, i.e., 100-1000 GHz. The use of solid state materials and phenomena, particularly for semiconductors, has become increasingly important in this direction. One principal semiconductor phenomenon which has been explored for use in MM and SMM control components is the solid state plasma state. Derived from this state are controllable conductive and dielectric properties which, in turn, are useful in controlling MM and SMM transmission and propagation. Furthermore, with the application of a static magnetic field, magnetized solid state plasmas exhibit a variety of interesting and potentially useful effects. Studies of electromagnetic (EM) wave interaction with magnetized semiconductor plasmas have revealed a number of specific physical properties which may be used for device purposes.

In this work, we study first the propagation characteristic of SMM waves in one-dimensional insulated image guide structures. The dispersion characteristics exhibit non-reciprocity which is essential for non-reciprocal device design. Feasibility studies performed on canonical models pertinent to the design of non-reciprocal devices such as isolators and differential phase shifters yielded highly encouraging results. Therefore we proceeded to an

INSTRUCTIONS FOR PREPARATION OF REPORT DOCUMENTATION PAGE

RESPONSIBILITY. The controlling DoD office will be responsible for completion of the Report Documentation Page, DD Form 1473, in all technical reports prepared by or for DoD organizations.

CLASSIFICATION. Since this Report Documentation Page, DD Form 1473, is used in preparing announcements, bibliographies, and data banks, it should be unclassified if possible. If a classification is required, identify the classified items on the page by the appropriate symbol.

COMPLETION GUIDE

General. Make Blocks 1, 4, 5, 6, 7, 11, 13, 15, and 16 agree with the corresponding information on the report cover. Leave Blocks 2 and 3 blank.

Block 1. Report Number. Enter the unique alphanumeric report number shown on the cover.

Block 2. Government Accession No. Leave Blank. This space is for use by the Defense Documentation Center.

Block 3. Recipient's Catalog Number. Leave blank. This space is for the use of the report recipient to assist in future retrieval of the document.

Block 4. Title and Subtitle. Enter the title in all capital letters exactly as it appears on the publication. Titles should be unclassified whenever possible. Write out the English equivalent for Greek letters and mathematical symbols in the title (see *"Abstracting Scientific and Technical Reports of Defense-sponsored RDT/E," AD-667 000).* If the report has a subtitle, this subtitle should follow the main title, be separated by a comma or semicolon if appropriate, and be initially capitalized. If a publication has a title in a foreign language, translate the title into English and follow the English translation with the title in the original language. Make every effort to simplify the title before publication.

Block 5. Type of Report and Period Covered. Indicate here whether report is interim, final, etc., and, if applicable, inclusive dates of period covered, such as the life of a contract covered in a final contractor report.

Block 6. Performing Organization Report Number. Only numbers other than the official report number shown in Block 1, such as series numbers for in-house reports or a contractor/grantee number assigned by him, will be placed in this space. If no such numbers are used, leave this space blank.

Block 7. Author(s). Include corresponding information from the report cover. Give the name(s) of the author(s) in conventional order (for example, *John R. Doe* or, if author prefers, *J. Robert Doe*). In addition, list the affiliation of an author if it differs from that of the performing organization.

Block 8. Contract or Grant Number(s). For a contractor or grantee report, enter the complete contract or grant number(s) under which the work reported was accomplished. Leave blank in in-house reports.

Block 9. Performing Organization Name and Address. For in-house reports enter the name and address, including office symbol, of the performing activity. For contractor or grantee reports enter the name and address of the contractor or grantee who prepared the report and identify the appropriate corporate division, school, laboratory, etc., of the author. List city, state, and ZIP Code.

Block 10. Program Element, Project, Task Area, and Work Unit Numbers. Enter here the number code from the applicable Department of Defense form, such as the DD Form 1498, "Research and Technology Work Unit Summary" or the DD Form 1634, "Research and Development Planning Summary," which identifies the program element, project, task area, and work unit or equivalent under which the work was authorized.

Block 11. Controlling Office Name and Address. Enter the full, official name and address, including office symbol, of the controlling office. *(Equates to funding sponsoring agency. For definition see DoD Directive 5200.20, "Distribution Statements on Technical Documents.")*

Block 12. Report Date. *Enter here the day, month, and year or month and year as shown on the cover.*

Block 13. Number of Pages. Enter the total number of pages.

Block 14. Monitoring Agency Name and Address *(if different from Controlling Office).* For use when the controlling or funding office does not directly administer a project, contract, or grant, but delegates the administrative responsibility to another organization.

Blocks 15 & 15a. Security Classification of the Report: Declassification/Downgrading Schedule of the Report. Enter in 15 the highest classification of the report. If appropriate, enter in 15a the declassification/downgrading schedule of the report, using the abbreviations for declassification/downgrading schedules listed in paragraph 4-207 of DoD 5200.1-R.

Block 16. Distribution Statement of the Report. Insert here the applicable distribution statement of the report from DoD Directive 5200.20, "Distribution Statements on Technical Documents."

Block 17. Distribution Statement *(of the abstract entered in Block 20, if different from the distribution statement of the report).* Insert here the applicable distribution statement of the abstract from DoD Directive 5200.20, "Distribution Statements on Technical Documents."

Block 18. Supplementary Notes. Enter information not included elsewhere but useful, such as: Prepared in cooperation with . . . Translation of *(or by)* . . . Presented at conference of . . . To be published in . . .

Block 19. Key Words. Select terms or short phrases that identify the principal subjects covered in the report, and are sufficiently specific and precise to be used as index entries for cataloging, conforming to standard terminology. The DoD "Thesaurus of Engineering and Scientific Terms" *(TEST)*, AD-672 000, can be helpful.

Block 20. Abstract. The abstract should be a brief *(not to exceed 200 words)* factual summary of the most significant information contained in the report. If possible, the abstract of a classified report should be unclassified and the abstract to an unclassified report should consist of publicly-releasable information. If the report contains a significant bibliography or literature survey, mention it here. For information on preparing abstracts see "Abstracting Scientific and Technical Reports of Defense-Sponsored RDT&E," AD-667 000.

☆ U.S. GOVERNMENT PRINTING OFFICE : 1973—729-091/1431 3-1

analysis of more practical structures, for example, the H-guide structures which have two-dimensional transverse cross-sections. It was found that only hybrid TE-TM modes exist and true surface waves propagate at frequencies above particular cutoff frequencies. The effect of semiconductor loss, dielectric loading, and structural parameters on the dispersion characteristics have also been investigated.

In addition to the non-reciprocal waveguiding property, GaAs materials also exhibit significant optical nonlinearity which allows frequency conversion. The nonlinearity is enhanced by the presence of electron plasmas in the medium. We therefore explored the role of solid state plasmas in nonlinear mixing schemes. In particular, the difference frequency generation of MM waves by two CO_2 lasers in a multilayer planar structure. The efficiency of power conversion is approximately of the same order of magnitude as that of a corresponding semiconductor bulk device. The effect of a biasing magnetic field on the nonlinear process is also investigated. It provides a means for phase matching as well as the enhancement of the power conversion efficiency.

Finally, we discuss practical experimental considerations which apply to the excitation and propagation of the surface plasma waves in a basic one interface structure. Current materials status appears to favor GaAs as the main candidate because of the high mobilities which have been reached to date in this semiconductor at cryogenic

temperatures (77K). The coupling of SMM radiation to a surface plasma waveguide has also been attempted by using a far infrared laser; however, this has been hampered by the lack of spatially clean transverse laser beam structure.

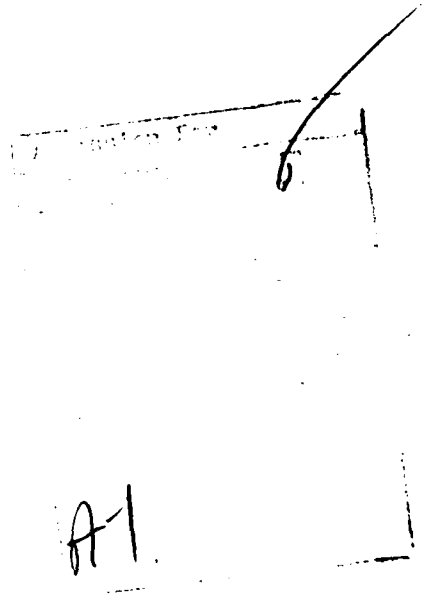

A-1

Table of Contents

List of Figures

1. Brief Review of Solid State Plasmas

1.1 Definition

In conductors and semiconductors there exist large numbers of free charge carriers. When the population densities of such charge carriers are sufficiently large, a situation arises where closest neighbor interactions dominate the behavior of the individual charge carriers. In addition to this shielding phenomenon, the dense cloud of charged particles also exhibit oscillation phenomena when an electric field is applied. The electrons and ions are accelerated in opposite directions and tend to separate. However strong electrostatic restoring forces are set up by this charge separation. Collective oscillations occur, i.e., the so-called plasma oscillations. The word 'plasma' is used to distinguish the collective behavior of charged particles from the individual behavior of the particles.

The shielding and oscillation characteristics of plasmas are described by two parameters, the 'Debye (or Thomas-Fermi) screening length (λ_D)' and the 'plasma frequency (ω_p)'. Both parameters depend crucially on the plasma density. In a moderately doped n-GaAs medium with, for example, $n_0 \sim 2.1 \times 10^{15} cm^{-3}$, the plasma frequency is given by (MKS unit)

$$\omega_p^2 = (n_0 e^2 / m^* \varepsilon_0) = 10^{13}/sec \qquad (1.1.1)$$

where

n_0= plasma concentration

e = electron charge

m^*= effective electron mass

ε_0= permittivity of free space

The screening length is given by

$$\lambda_D=(2\varepsilon_0\varepsilon_F/3n_0e^2)^{1/2} = 230\text{Å} \qquad (1.1.2)$$

where

ε_F = Fermi energy

Note that for this solid state plasmas $\lambda_D n_0^{1/3}<1$ which is very different from the condition $\lambda_D n_0^{1/3}>>1$ imposed by the gaseous plasmas. However, in this range of concentration, the semiconductor exhibits collective behavior and is still considered to be in the plasma state[1].

Another important plasma parameter is the collision frequency. In an applied electric field, electrons or holes drift parallel to the field. However, they can lose their acquired drift velocity through collisions. If the collision frequency is high compared to the frequency of the applied fields, electrons do not have enough time to accelerate and decelerate between collisions. Thus, apart from a high frequency jitter, there is no separation of charges. The system then behaves as a lossy conductor. On the other hand, if the collision frequency is small compared to the frequency of the applied fields, the charge separation must be considered and the

system is in the plasma state. In doped semiconducting media, the collision frequency is determined by two major scattering mechanisms, namely, impurity scattering and lattice phonon scattering. The probability of impurity scattering increases with the concentration of ionized impurities and the probability of phonon scattering increases with lattice temperature. Clearly, cooling will reduce the phonon scattering phenomenon. At liquid nitrogen temperature ($77^{\circ}K$), high quality GaAs material with $n_0 \sim 2.1 \times 10^{15} cm^{-3}$ can have a collision frequency in the range of 10^{11} Hz. This corresponds to a momentum relaxation time of 10^{-11} sec and an electron mobility of $\sim 10^5 cm^2/V\text{-sec}$.

1.2 EM Wave-Solid State Plasma Interaction

Consider an EM wave propagating inside a homogeneous, moderately doped GaAs medium. In the MM and SMM wave range, the interaction of conduction electrons with the applied EM field is well described by the plasma theory. The equation of motion for a free electron is given by

$$\partial \underline{v}/\partial t + (\underline{v} \cdot \nabla)\underline{v} + \nu \underline{v} = (e/m^*)(\underline{E} + \underline{v} \times (\underline{B} + \underline{B}_0)) \qquad (1.2.1)$$

where

$\underline{v}$ = electron velocity

ν = collision frequency

Here we have assumed that a d.c. magnetic field $\underline{B}_0$ is applied to the plasma medium. The above equation includes second order terms such

as the Lorentz force term $\underline{v}X\underline{B}$ and the term $(\underline{v}\cdot\nabla)\underline{v}$. The latter is part of a convective derivative of $\underline{v}$, i.e., $d\underline{v}/dt = \partial\underline{v}/\partial t + (\underline{v}\cdot\nabla)\underline{v}$, which gives the total rate of change of quantities moving with the instantaneous velocity $\underline{v}$. These second order terms (nonlinear effects) will be discussed in more detail in Chapter 3 where we examine the use of electronic plasmas in nonlinear generation schemes. Here we only look for the first order effects. Through the equation that relates the current density to the carrier velocity, i.e.,

$$\underline{J} = -ne\underline{v} = \sigma(\omega)\underline{E} \tag{1.2.2}$$

the solution of equation (1.2.1) yields the conductivity tensor. This result can also be expressed in terms of a permittivity tensor. For a biasing magnetic field in the $\hat{y}$-direction, the tensor takes the following form[2]:

$$\varepsilon(\omega) = \begin{bmatrix} \xi & 0 & -j\eta \\ 0 & \zeta & 0 \\ j\eta & 0 & \xi \end{bmatrix} \tag{1.2.3}$$

where

$$\xi = \varepsilon^{(0)} - \frac{\omega_p^2(\omega - j\nu)}{\omega[(\omega - j\nu)^2 - \omega_c^2]} \tag{1.2.4}$$

$$\zeta = \varepsilon^{(0)} - \frac{\omega_p^2}{\omega(\omega - j\nu)} \tag{1.2.5}$$

$$\eta = \frac{-\omega_p^2\omega_c}{\omega[(\omega - j\nu)^2 - \omega_c^2]} \tag{1.2.6}$$

$\varepsilon^{(0)}$ = static dielectric constant

ω_c = cyclotron frequency

ν = collision frequency

Note the asymmetrical property of this tensor. It characterizes a gyroelectric material which, analogous to gyromagnetic material, can lead to device designs which exhibit non-reciprocity.

2. Nonreciprocal Components Using Magnetoplasmons on Semiconducting Substrates

For thirty years, non-reciprocal component such as differential phase shifters, isolators and circulators have played a crucial role in the design of circuits and systems from L band through K band. These several component types have yielded systems with very impressive performance characteristics both in discrete as well as hybrid forms and, in recent years, been used in integrated configurations. The most crucial aspect was the development of very high quality ferrite materials suitable for use at frequencies as low as hundreds of MHz (i.e., L band) to as high as the tens of GHz in the K_u to K_a bands. Rare earth ferrites and garnet materials have allowed the design and construction of devices with reasonable, even acceptable, performance in the 94 GHz band. However, as we move to the SMM range, ferrite technology will be unlikely to see use in the design of non-reciprocal components because of high loss. Alternative technologies are required if we are to have available the flexibility and sophistication now possible using ferrite loaded devices at lower frequencies. In 1980, Nurmikko and Bolle[3] proposed the use of surface plasmon modes supported on appropriately doped high quality semiconducting substrates as a potential solution. These electromagnetic modes coupled to the solid state plasma, and subject to a d.c. magnetizing field, provide a modal hierarchy exhibiting strong non-reciprocal effects.

To design magnetoplasmon-based non-reciprocal devices, we need to understand first appropriate dispersion characteristics. The propagation of surface magnetoplasmons along the interface between two semi-infinite media, one of which may be a metal or semiconductor, have seen extensive investigation both theoretically and experimentally[4-7]. Of the many possible geometries, we shall consider only the Voight configuration in which the applied magnetic field is normal to both the principal electric field component and the direction of propagation. Investigations of a class of basic canonical structures have been reported. These give insight into the performance characteristics of elemental differential phase shifters and non-reciprocal isolators[8]. In these early studies the geometries considered consist of single and multiple interfaces. That is, a single dielectric-semiconductor interface or slabs of semiconducting material, single or double and loaded by dissimilar dielectric media on either side and/or interspersed between the semiconducting layers. Performance predictions based on a 5-region canonical structure were reported[9] for isolators and differential phase shifters in the SMM wave range. Sample results showed the possibility of acceptable performance for isolators over a bandwidth of 45 GHz in the 500 GHz range and of differential phase shifter design over a bandwidth of 65 GHz in the 380 GHz range. However, for differential phase shifters, significant non-reciprocal phase shifts ($\approx 80^{\circ}$-120°/mm) at sufficiently low values of insertion loss

(<0.76 dB/mm) can only be obtained for improved relaxation times (i.e., $\tau \simeq 2.0 \times 10^{-12}$ sec) than those currently available.

To obtain high performance devices with available materials, we explore new canonical structures as well as optimization of design. In section 1 of this chapter, the propagation characteristic of magnetoplasmons in an insulated image guide structure is studied and the performance of SMM wave isolators and phase shifters is evaluated. To refine our model and so approach more closely practical geometrical structures, we examine in Section 2 the H-guide structure which has a finite transverse cross-section. The analysis and results have also been reported in references 10 and 11.

2.1 Insulated Image Guide Structures

2.1.1 Wave Propagation

The structure to be analyzed is depicted in Fig. 1. It is a one-dimensional structure which consists of a magnetized GaAs slab (region 2) parallel to but separated from a perfectly conducting plane by an isotropic dielectric region (region 1). In the presence of solid state plasmas, the macroscopic fields of a propagating wave can be obtained from Maxwell's equations:

$$\nabla \times \underline{E} = -j\omega\mu_0 \underline{H}$$
$$\nabla \times \underline{H} = j\omega\varepsilon_0 \underline{\underline{\varepsilon}} \cdot \underline{E} \qquad (2.1.1)$$
$$\nabla \cdot \underline{H} = 0$$
$$\nabla \cdot \underline{D} = \nabla \cdot (\varepsilon_0 \underline{\underline{\varepsilon}} \cdot \underline{E}) = 0$$

Here, a time dependence factor $e^{j\omega t}$ has been assumed. Two coupled equations for the transverse electric and magnetic field E_y and H_y can be deduced from these equations, assuming a propagation factor $e^{-\gamma z}$:

$$\frac{\partial^2 E_y}{\partial x^2} + (k_0^2 \zeta + \gamma^2) E_y + \frac{\zeta \partial^2 E_y}{\xi \partial y^2} = \frac{-\omega\mu\eta}{\xi} \frac{\partial H_y}{\partial y} \qquad (2.1.2)$$

$$\frac{\partial^2 H_y}{\partial x^2} + (k_0^2 \varepsilon_e + \gamma^2) H_y + \frac{\partial^2 H_y}{\partial y^2} = \frac{\omega\mu\eta}{\xi} \frac{\partial E_y}{\partial y} \qquad (2.1.3)$$

where

$$\varepsilon_e = (\xi^2 - \eta^2)/\xi \qquad (2.1.4)$$

All the field components transverse to the $\hat{y}$-axis can be expressed in terms of E_y anf H_y:

$$(\gamma_1^4 - k_0^4 \eta^2) \underline{E}_t$$
$$= \gamma_1^2 j\omega\mu \hat{y} \times \nabla_t H_y + k_0^2 \omega\mu\eta \nabla_t H_y + \gamma_1^2 \nabla_t \frac{\partial E_y}{\partial y} + jk_0^2 \eta \hat{y} \times \nabla_t \frac{\partial H_y}{\partial y} \qquad (2.1.5)$$

$$(\gamma_1^4 - k_0^4 \eta^2) \underline{H}_t$$
$$= \gamma_1^2 \nabla_t \frac{\partial H_y}{\partial y} + jk_0^2 \eta \hat{y} \times \nabla_t \frac{\partial H_y}{\partial y} + \omega\eta\varepsilon_0 \nabla_t \frac{\partial^2 E_y}{\partial y^2} - j\omega\varepsilon_0 \zeta \gamma_2^2 \hat{y} \times \nabla_t E_y \qquad (2.1.6)$$

where

$$\gamma_1^2 = k_0^2 \xi + \partial^2/\partial y^2$$

$$\gamma_2^2 = k_0^2 \varepsilon_e + \partial^2/\partial y^2$$

$$\nabla_t = \hat{x}\partial/\partial x - \hat{z}$$

Since $\partial/\partial y = 0$, the solution of eqs. (2.1.2) and (2.1.3) can be decomposed into pure TE or TM modes which have nonzero field components E_y, H_x, H_z and H_y, E_x and E_z, respectively. Of the two possible modes, only TM modes are considered here since fields corresponding to TE modes do not show interesting interactions with the semiconducting material. The electric polarization of the TM type of waves lies in the plane transverse to the applied magnetic field. Therefore, in addition to the plasma oscillation, the electrons also precess about the applied magnetic field. As a result, we get an effective dielectric constant ε_e which is defined by eq. (2.1.4). It is a function of the cyclotron frequency, the plasma frequency and the frequency of the propagating wave. Fig. 2 shows a plot of the effective dielectric constant as a function of frequency. The critical frequencies[8] $\omega_0^{(1)}$, $\omega_0^{(2)}$ and ω_∞ define regions where $\varepsilon_e < 0$. It is in these frequency bands that the bounded surface waves exist which have exponentially decaying fields in the transverse direction, away from the guiding structure. We then, in the semiconductor region, seek a solution of eq. (2.1.3), together with other field components, in the form:

in region 2

$$H_{y2} = Ae^{-k_2(x-T)} + Be^{k_2(x-T)}$$
$$E_{z2} = (j/\omega\varepsilon_e\varepsilon_0)[A(k_2^+)e^{-k_2(x-T)} - B(k_2^-)e^{k_2(x-T)}]$$
$$E_{x2} = (1/\omega\varepsilon_e\varepsilon_0)[-A(k_2'^+)e^{-k_2(x-T)} - B(k_2'^-)e^{k_2(x-T)}] \quad (2.1.7)$$

where

$$-k_2^2 - \gamma^2 = k_0^2\varepsilon_e \quad (2.1.8)$$

and

$$k_2^{\pm} = k_2 \pm j\gamma\eta/\xi$$
$$k_2'^{\pm} = k_2\eta/\xi \pm j\gamma$$

Similarly, in the isotropic dielectric regions, the field components are given by:

in region 1

$$H_{y1} = C(e^{-k_1 x} + e^{k_1 x})$$
$$E_{z1} = (jk_1/\omega\varepsilon_1\varepsilon_0)C(e^{-k_1 x} - e^{k_1 x}) \quad (2.1.9)$$
$$E_{x1} = (-j\gamma/\omega\varepsilon_1\varepsilon_0)H_{y1}$$

where

$$-k_1^2 - \gamma^2 = k_0^2\varepsilon_1 \quad (2.1.10)$$

in region 3

$$H_{y3} = e^{-k_3(x-T-W)}$$
$$E_{z3} = (jk_3/\omega\varepsilon_3\varepsilon_0)e^{-k_3(x-T-W)} \quad (2.1.11)$$
$$E_{x3} = (-j\gamma/\omega\varepsilon_3\varepsilon_0)H_{y3}$$

where

$$-k_3^2 - \gamma^2 = k_0^2 \varepsilon_3 \qquad (2.1.12)$$

The unknown coefficients A,B,C and the propagation constant can be obtained through applying the appropriate boundary conditions, e.g., H_y and E_z must be continuous at the x=T and x=T+W planes. This results in a complex transcendental equation:

$$e^{-2k_2 W} = \frac{[\varepsilon_e k_1 \tanh(k_1 T) + \varepsilon_1 k_2^+][\varepsilon_e k_3 + \varepsilon_3 k_2^-]}{[\varepsilon_e k_1 \tanh(k_1 T) - \varepsilon_1 k_2^-][\varepsilon_e k_3 - \varepsilon_3 k_2^+]} \qquad (2.1.13)$$

At a given frequency, the complex propagation constant is obtained using a HP-1000 computer and an algorithm based on Davidenko's method. This algorithm has been reported in detail in reference (2).

Theoretical dispersion curves have been obtained for surface magneto-plasmons where the effects of both damping and retardation have been included. Throughout this chapter, calculations are shown which use values of parameters appropriate for n-type GaAs, i.e., $\varepsilon^{(0)}=13$, $|\omega_c/\omega_p|=0.1$, $\nu=0$ or $\omega_p/80$, and $\omega_p=10^{13}$/sec. Here we want to emphasize the fact that all frequency terms can be normalized with respect to ω_p, the plasma frequency. All dielectrics are considered loss free but the semiconductor can be considered either loss free or lossy.

Consider first a single interface structure with two semi-

infinite media: air and lossless GaAs. The criterion for 'true' bounded surface wave propagation along the interface is that the wave amplitude must decay exponentially away from the interface. Mathematically, this means that the values of k_2 in eq. (2.1.8) and k_3 in eq. (2.1.12) must be real. These two equations with $k_2^2=0$ and $k_3^2=0$ thus define dispersion curves which separate the surface wave region from the 'bulk magnetoplasmon' region and the 'radiation' region, respectively. In the bulk magnetoplasma region, the propagating waves become volume modal waves. The propagation constant assumes complex value even if the dielectric loss is neglected for both the air and the GaAs regions. Its real part, α, represents propagation normal to the surface which produces a loss of energy, i.e., radiation from the surface into the interior of the semiconductor. When the semiconductor loss is taken into consideration, these volume modal waves suffer additional attenuation from its sinusoidal field distribution within the lossy GaAs slab. In the radiation region, the wave radiates in the transverse direction and decays exponentially in the longitudinal direction.

Surface waves propagating in opposite directions experience different dispersion effects. This same phenomenon can also be obtained by reversing the direction of the applied magnetic field. This non-reciprocity is manifested by the first order linear term in γ in the transcendental equation. This phenomenon can be utilized

for non-reciprocal isolator and differential phase shifter designs. In Fig. 3 two branches were found for both directions of propagation. The lower branch approaches the light line asymptotically at the low frequency end. At the high frequency end, it terminates at the intersection with the 'bulk' magnetoplasmon dispersion curve when $\omega_c>0$ (forward direction of propagation) and it also approaches the asymptotic frequency for the unretarded surface magnetoplasmons when $\omega_c<0$. This unretarded surface magnetoplasmon frequency is defined by

$$\omega_s^{(1,2)}=\left[\ \omega_c \mp \sqrt{\omega_c^2+4\omega_p^2/(\varepsilon^{(0)}+\varepsilon_3)}\right]/2 \qquad (2.1.14)$$

and is sometimes referred to as the surface magnetoplasma frequency. For the upper branch, when $\omega_c>0$, the dispersion curve begins at the light line at the point where $\xi=0$ and it terminates when entering into the bulk magnetoplasmon dispersion region. For $\omega_c<0$, the dispersion curve begins at the light line at the point where $\xi=\varepsilon_1=1$ and as the frequency increases it asymptotically approach the unretarded surface mangetoplasmon frequency which, in this case, is obtained from eq. (2.1.14) by replacing ε_3 with ε_1. Also shown on the same figure is the surface magnetoplasmon dispersion curve for the dielectric-GaAs interface. There is only one branch for the forward direction of propagation, while for the reverse direction of propagation two branches are obtained. Backbends are observed when damping is present[12].

When two single interface structures are placed side by side, we obtain a single slab structure. The surface wave mode of the composite structure results from the coupling between the individual interface waves[8]. For the asymmetrically loaded single slab structure, that is, a semiconducting slab sided by differing dielectric media, 'true' surface waves exist in the ω-β diagram only to the right of the light line associated with the high dielectric region. However, for some choice of parameters, we do find the existence of surface wave to the left of the high-dielectric light line. For example, in Figs. 4a and 4b, we find that the S mode exist between the $\omega=k_0c$ and $\omega=k_0c\sqrt{\varepsilon_1}$ light lines. This is the mode which relates to the symmetrical (or even) modes of a symmetrically loaded single slab structure. However, it only exists for the forward direction of propagation. These surface plasmons are called 'generalized' modes[4] since they may have complex propagation constant even when the semiconducting material is considered loss free. Similar to the bulk magnetoplasmons, the 'generalized' surface waves also have a propagation component normal to the surface which carries energy away from the interface. If we increase the slab thickness, more energy radiates away from the interface and is trapped inside the semiconducting medium. The propagating wave suffers from the radiation loss. When significant material loss is present in the semiconducting medium, the wave suffers sufficient attenuation that it eventually vanishes. On the

other hand, if we decrease the slab thickness, more energy is forced to travel in the low dielectric region. The generalized surface waves thus change into space waves and we tend to reach the practical limit of our numerical method. Therefore, the generalized surface wave in practice can be observed only for a very limited range of the slab thickness and material loss.

The difficulties mentioned above no longer exist in the insulated image guide structures. The presence of a metallic wall on the high dielectric side does allow a 'non-radiating' sinusoidal wave to exist in that region. Thus a true surface wave can exist between the light lines of the low and high dielectric regions on the ω-β plane. In Fig. 5a and 5b we display, as a function of frequency, the solution for the transcendental equation for both directions of propagation. In these figures the short broken lines divide the surface magnetoplasma region from the bulk magnetoplasma region located in the frequency ranges between $f_0^{(1)}$ and f_∞ and above $f_0^{(2)}$. In the surface magnetoplasma region there exist, generally, three branches for either direction of propagation. In the lower frequency range we have, in additional to the S branch, an A branch which relates to the asymmetrical (or odd) modes of a symmetrically loaded single dielectric slab structure. In the higher frequency range, there exists a D branch which describes an electrodynamic mode similar to the magnetodynamic mode found on ferrite loaded wave guiding structure. In this frequency range

there also may exist a fourth branch, the electrostatic branch, which, however, is heavily attenuated and thus ignored.

2.1.2 Non-reciprocal Isolators

In the design of isolators, the most important parameters are the isolation ratio, the insertion loss and the bandwidth. As can be seen in Fig. 5a and 5b, the A branch for an insulated image guide structure suffers considerable attenuation and cannot be used in practical applications. The S branch, however, exhibits a non-reciprocal attenuation property which can be used as a basis for isolator design. The isolation obtained features finite bandwidth. On the low frequency side it is limited by the decreasing attenuation constants for both directions of propagation. Also, little non-reciprocity is observed here. On the high frequency side it is limited by the increasing insertion loss. This is caused by the fields gradually penetrating into the slab and becoming increasingly attenuated at high frequencies.

The three primary parameters that affect device performance are the GaAs slab width W, the dielectric slab thickness T and the dielectric constant ε_1. These parameters must be chosen properly to give the desired isolator characteristics. However, increasing the dielectric thickness by a factor of $\sqrt{N}$ has approximately the same effect on the attenuation and dispersion curves as increasing the dielectric constant by a factor of N. Hence, we will only discuss

the effect on the isolator characteristics of varying the two parameters W and ε_1.

Figure 6a illustrates, for the geometry shown in Fig. 1, the isolation ratio and insertion loss as functions of frequency for various GaAs slab width. At a given frequency, a wider semiconducting slab increases the non-reciprocity in the propagation characteristics, thus giving a higher isolation ratio. At the same time, the increase of the slab width yields a higher insertion loss and a trade-off is indicated.

Similarly, Fig. 6b shows that increasing the dielectric loading results in principally increasing the insertion loss, thus reducing the useful bandwidth.

From Fig. 6a and 6b we find that for W=25 μm, T=25 μm and ε_1=4, the geometry studied gives quite acceptable isolator behavior with an isolation ratio of 10:1 and an insertion loss of less than 0.5 dB/mm over a bandwidth of 65 GHz in the 400 GHz range. This is a 15% bandwidth and is an improvement over the result reported in ref. (9), where the same isolation characteristics were obtained over a 10% bandwidth for a five-region canonical structure.

2.1.3 Differential Phase Shifters

In Figs. 5a and 5b it shows that branch D, with a proper choice of the parameters, is suitable for differential phase shifter designs over wide bandwidths. Figure 7 shows the differential phase shift and insertion loss as functions of frequency for different device configurations. The low and high frequency limits are set by f_∞ and the insertion loss, respectively.

From Fig. 7 we see that for $\epsilon^{(0)}$=13, T=10 μm and W=25 μm, phase shifts of 35°/mm to 65°/mm while an insertion loss of less than 1 dB/mm can be obtained over a bandwidth of ~90 GHz centered at 550 GHz. The differential phase shift changes by less than 10% over a 30 GHz range, corresponding to a highly desirable slope of less than 0.5°/GHz.

In the design of differential phase shifters we would also like to have as large a phase shift/insertion loss ratio as possible over a reasonable bandwidth. Figure 8 shows the ratio of differential phase shift to insertion loss as a function of frequency for several device configurations of differing geometric dimensions. Curves of insertion loss as a function of frequency are also included on the same graph to indicate the limits on bandwidth set by the insertion loss.

From figure 8, we obtain a differential phase shift per dB loss

of about 75^{o}/dB for an 8% bandwidth. This is to be compared with the results reported in ref. (9) for the five region models. There a ratio of 100^{o}/dB is obtained over the same bandwidth. However, a higher quality GaAs material with $\tau = 20 \times 10^{-12}$ sec is required.

One final note is that for the two modes employed for isolation and phase shifting, i.e., branches S and D, respectively, most of the electromagnetic energy is guided along the GaAs-air interface and away from the conducting plane. Any loss in the conductor would have little impact on the attenuation and dispersion characteristics. The assumption of a loss free conducting plane is thus justified.

2.2 H-guide Structures

In the previous section, we studied the propagation of surface magneto-plasmon on the insulated image guide structures and the feasibility of using it as a basis for the non-reciprocal device applications. The structures involved are assumed to be uniform and invariant in the $\hat{y}$-direction which is parallel to the interface and perpendicular to the direction of propagation $\hat{z}$. The field distributions of the propagating TM modal waves are then uniform in the $\hat{y}$-direction. In practice, however, the guided wave would assume a finite and non-uniform transverse field distribution, hence higher order modes must be considered.

Here, an investigation of the dispersion characteristic is presented for an H-guide structure (Fig. 9) where the two parallel plates are taken to be electric walls and the rectangular slab of either infinite width (single-interface structure) or finite width (slab structure). The slab is chosen to be high quality, moderately doped n-type GaAs material. It is sided by two semi-infinite regions which have dielectric constants ε_1 and ε_3, respectively. The biasing magnetic field is applied in the $\hat{y}$-direction and is perpendicular to the electric walls and parallel to the normal of the sagittal plane (Voight configuration).

Electromagnetic wave propagation in this structure is governed by the Maxwell's equations. In the semiconductor region, the field distribution can be obtained from eqs. (2.1.2) to (2.1.6). However, for the two-dimensional model, eqs. (2.1.2) and (2.1.3) can no longer be decoupled. The presence of the electric walls introduces coupling between the TE and TM mode waves which greatly complicates the mathematics involved. Fortunately, the assumption of perfectly conducting planes enables the separation of variables. All field components have trigonometric distributions along the $\hat{y}$-direction. For example, the $\hat{y}$-component of the electric and magnetic field can be expressed as follows:

$$E_y(x,y) = e_y(x)\ \cos k_y y$$
$$H_y(x,y) = h_y(x)\ \sin k_y y \qquad (2.2.1)$$

where

$k_y = n\pi/h$ = transverse wave number

n = integer = order of mode

h = height of the structure

Substitution of eq. (2.2.1) into eqs. (2.1.2) and (2.1.3) yields the following coupled linear equations:

$$\frac{\partial^2 e_y}{\partial x^2} + (\frac{\zeta}{\xi}\gamma_1^2 + \gamma^2) e_y = - \frac{\omega\mu_0}{\xi} k_y h_y \qquad (2.2.2)$$

$$\frac{\partial^2 h_y}{\partial x^2} + (\gamma_2^2 + \gamma^2) h_y = - \frac{\omega\mu_0}{\xi} k_y e_y \qquad (2.2.3)$$

where

$$\gamma_1^2 = k_0^2 \xi - k_y^2$$
$$\gamma_2^2 = k_0^2 \varepsilon_e - k_y^2$$

The general solution for the above equations can be found in many texts[13]. The complex field strength amplitudes in the semiconducting region can be written as follows:

For $0 \leqslant x \leqslant W$

$$E_{y2} = (e^{\lambda_1 x} + Be^{-\lambda_1 x} + Ce^{\lambda_2 x} + De^{-\lambda_2 x}) \cos k_y y$$

$$H_{y2} = q_1 (e^{\lambda_1 x} + Be^{-\lambda_1 x}) + q_2 (Ce^{\lambda_2 x} + De^{-\lambda_2 x}) \sin k_y y$$

$$E_{z2} = (A_1 e^{\lambda_1 x} + BB_1 e^{-\lambda_1 x} + CC_1 e^{\lambda_2 x} + DD_1 e^{-\lambda_2 x}) \sin k_y y$$

$$H_{z2} = (A_2 e^{\lambda_1 x} + BB_2 e^{-\lambda_1 x} + CC_2 e^{\lambda_2 x} + DD_2 e^{-\lambda_2 x}) \cos k_y y$$

$$E_{x2} = (A_3 e^{\lambda_1 x} + BB_3 e^{-\lambda_1 x} + CC_3 e^{\lambda_2 x} + DD_3 e^{-\lambda_2 x}) \sin k_y y$$

$$H_{x2} = (A_4 e^{\lambda_1 x} + BB_4 e^{-\lambda_1 x} + CC_4 e^{\lambda_2 x} + DD_4 e^{-\lambda_2 x}) \cos k_y y$$

where

$$\lambda_{1,2}^2 = -\gamma^2 - \frac{1}{2\xi}\left(\zeta\gamma_1^2+\xi\gamma_2^2 \pm RT\right) \tag{2.2.4}$$

$$RT = \left[(\zeta\gamma_1^2-\xi\gamma_2^2)^2 + 4k_o^2\zeta\eta k_y^2\right]^{1/2} \tag{2.2.5}$$

and

$$q_{1,2} = \left[(\xi\gamma_2^2-\zeta\gamma_1^2)\pm RT\right]/(2\omega\mu\eta k_y) \tag{2.2.6}$$

Here, $\{A_i, B_i, C_i, D_i\}$, i=1 to 4 are known functions of γ and B, C, D are unknown coefficients of the field distribution.

If k_y=0, as in the one-dimensional case, eq. (2.2.4) is reduced to the dispersion equation of the TE or TM modes, respectively. The normal modes of the propagating wave thus can be separated into pure TE or TM modes.

In the isotropic dielectric regions, the field distribution takes a simpler form:

For $x \leqslant 0$

$$E_{y1} = Ee^{k_1 x}\cos k_y y$$

$$H_{y1} = Fe^{k_1 x}\sin k_y y$$

$$E_{z1} = (E_1 E+F_1 F)e^{k_1 x}\sin k_y y$$

$$H_{z1} = (E_2 E+F_2 F)e^{k_1 x}\cos k_y y$$

$$E_{x1} = (E_3 E+F_3 F)e^{k_1 x}\sin k_y y$$

$$H_{x1} = (E_4 E+F_4 F)e^{k_1 x}\cos k_y y$$

with $\quad -k_1^2+k_y^2-\gamma^2 = k_0^2\varepsilon_1 \qquad (2.2.7)$

Again, $\{E_i, F_i\}$, i=1 to 4 are known functions of γ and E, F are unknown coefficients.

For x≥W, similar field expressions are obtained by replacing k_1 and ε_1 with $-k_3$ and ε_3 and E_1, F_1, E, F by another set G_1, H_1, G, H.

Matching the boundary conditions at x=0 and W, we can solve for the complex propagation constant and the coefficients of the field distributions.

Let us consider first a single interface H-guide structure consisting of semi-infinite air and GaAs media. The lowest order mode (k_y=0) is TM in nature and it has a uniform field distribution in the y-direction. Its dispersion curve exhibits the same phenomena as those given in Fig. 3 as well as those reported on previously[5,8].

If the semiconducting medium is loss free, the propagation constant $\gamma = \alpha + j\beta$ for the lowest order surface wave mode is purely

imaginary. It represents a 'true' bounded surface wave which propagates unattenuated. The higher order modes, however, may have complex propagation constant and thus become generalized surface wave modes. Figure 10 shows a relationship between the frequency and the transverse wave number k_y. The curve is defined by RT=0 (eq. 2.2.5) which separates the 'true' surface wave region from the 'generalized' surface wave region. For a given frequency, 'true' surface wave propagation occurs for modes with k_y values outside the shaded region. However, a very large k_y/k_0 value implies that $\lambda_{1,2}/k_0$ and k_1/k_0 also have to be large and the surface wave cannot exist even within the immediate vicinity of the interface. Thus at a given frequency, only those surface wave modes with k_y less than a certain value can propagate in the 'generalized' sense. And for a specified mode, i.e., for a given k_y value, increasing attenuation occurs as the frequency decreases and eventually the mode becomes evanescent.

The loss and dispersion curves for the higher order surface magnetoplasmons of a single-interface H-guide structure are given in Fig. 11a. Here we have also included the loss effect of the semiconducting medium. There is only one branch for either direction of propagation. At the high frequency end, the dispersion curve of the forward-going wave extends into the bulk magnetoplasma region where $\lambda_{1,2}^2<0$ while the loss curve (long broken line) leads into high attenuation range where practical application is limited.

For the reverse direction, the wave ceases to propagate as the attenuation (indicated by the dotted line) becomes excessive. This is also demonstrated by the bendover of the dispersion curve. At the low frequency end, note the sharp increase in attenuation below cutoff. The cutoff frequency increases as k_y increases. For those modes where the cutoff frequency becomes equal to or greater than the surface magnetoplasma frequency, the surface wave ceases to exist. This point is illustrated by a special example shown in Fig. 11b. In the reverse direction of propagation, the normalized cutoff frequency for the normal mode of a single interface structure is around .22 which is very close to the surface magnetoplasma frequency $\omega_s^{(1)}$ which is shown in Fig. 3. Therefore wave propagation is being cutoff in the reverse direction and the propagation becomes unidirectional.

If the semiconductor region is thin enough, there will be strong coupling between the surface waves that propagate on both surfaces of the slab. The H-guide structure in which we are interested is such a case. In Fig. 11a, we use solid lines to illustrate the dispersion curve for the symmetrically loaded, i.e., $\varepsilon_1=\varepsilon_3$, H-guide structures. It has two branches, S and A, both of which are symmetric about the frequency axis and lie very close to the single interface dispersion curve. As the slab becomes even thinner, branch S moves closer toward the light line, i.e., more energy travels outside the semiconductor region and the attenuation

decreases. However for branch A, in the case of a thinner slab, more energy is trapped inside the semiconducting slab. The dispersion curve moves away from the light line and the attenuation increases.

In a practical structure, the semiconductor slab has to be supported by some kind of substrate. Thus it is loaded asymmetrically by differing dielectrics on either side. A typical dispersion diagram for such a structure is depicted by the solid lines in Fig. 11b. Generally no bounded modes can exist in the region of the ω-β plane which is to the left of the $k_1^2=0$ line. The dispersion curve has two branchs, S and A, in the forward direction of propagation and only one branch, A, in the reverse direction of propagation. The attenuation for the A branch is slightly lower for those modes with higher value of k_y, while for the S branch it is slightly higher. The attenuation for both modes can be reduced if the dielectric constant of region 1 is made smaller.

Checking the field distribution, we find a similar field displacement effect for the symmetrically loaded, single slab H-guide structure as that reported on previously[8] for its 1-dimensional counter part. We also find that at low frequencies, the amplitude of the transverse electric field, E_y, is far greater than that of the longitudinal field, E_z. That is, the surface plasmon is predominantly of the TE type and there is little interaction with the semiconductor material. At high frequencies, however, $H_y>>H_z$,

the TM aspect predominates and strong interaction with the anisotropic semiconductor is evidenced by the highly non-reciprocal dispersion curve. This non-reciprocity can be used as a basis for the design of isolators and differential phase shifters.

In conclusion, the surface wave propagation in the insulated image guide structures and H-guide structures have been investigated. Understanding how surface magnetoplasmons propagate along a single dielectric-semiconductor interface and how two surface magnetoplasmons on different interfaces couple to each other, we can readily predict the dispersion properties of more complicated structures and obtain fairly accurate assessments of possible device performance.

3. Nonlinear Generation of Surface Plasmons on Planar Structures

Solid state plasmas exhibit nonlinear polarizability which makes frequency conversion possible. Considerable interest exists in the nonlinear generation of millimeter and submillimeter waves so as to provide potentially tunable sources in the 100 to 1000 GHz range. The nonlinear generation method may also be used for the excitation of surface magnetoplasmons. which, as was mentioned in Chapter 2, can be utilized in non-reciprocal device design. In the past twenty years there have been intensive efforts among scientists to exploit the phenomena of nonlinear optics for down conversion of the signal frequency generated by tunable CO_2 lasers. The CO_2 gas laser is very appropriate for this application since it combines high power output with many discrete frequencies of oscillation in the range $9\sim11$ μm. Possible differences between two such frequencies can range from 150-4000 GHz while high spectral purity with bandwidth of $\sim$100 KHz may be obtained[14,15].

The basic theory of optical mixing in a crystal is well known. The interaction of propagating optical waves in a nonlinear medium induces a distribution of electric dipoles which radiate EM waves at the sum, difference or harmonic frequencies of the input waves. In the difference frequency generation case, this nonlinear polarization has a phase factor $e^{j(\Delta\omega t-\Delta k_z z)}$ which is determined by the relative phase of the input waves. It is sometimes referred to

as the 'polarization wave'[16]. And since this polarization wave will generate, or drive, EM waves at the same frequency, it is also called a driving wave. In this chapter, the name driving wave and polarization wave will be used interchangeably, as will the name of driven wave and output wave.

To produce a favored output at the difference frequency it is necessary to have an optical material with significant polarization nonlinearity for the input frequency. However, the nonlinearity of existing materials is not sufficient to give significant mixing except over distances much greater than the signal wavelength. As a result, crystals available in relatively large sizes are preferred and phase matching, which permits the coherent generation of output wave over a long interaction path, must be maintained.

GaAs is one of the most popular materials in such an application. It has a relatively large nonlinear coefficient at optical frequencies and small absorption loss at both the optical and SMM wave frequencies. Neglecting the effect of absorption and boundary refraction, the maximum output power for the phase-matching operation can be obtained[17]:

$$P_3 = \sqrt{\frac{\mu_0}{\varepsilon_0}}\,\frac{(\omega_3)^2(2d)^2L^2}{2n_1n_2n_3c^2}\left(\frac{P_1P_2}{A}\right)R_1R_2R_3\left[\mathrm{sinc}(\Delta k_z L/2)\right]^2 \qquad (3.1.1)$$

where

$\omega_{1,2}$= frequency of the input waves

ω_3 = frequency of the output wave

2d = nonlinear optical susceptibility

L = crystal length over which the beams mix

c = light velocity

A = area of the beam cross-section

$n_{1,2,3}$=refractive indices at $\omega_{1,2,3}$, respectively

$P_{1,2,3}$=input power at the respective frequencies

$R_{1,2,3}$=single surface transmission coefficients at frequencies $\omega_{1,2,3}$, respectively

sinc(x)=sin x/x

The efficiency of the power conversion is low. So far, the best that has been achieved with pulsed input power in the 100 KW to 1 MW range are far-infrared outputs with peak powers in the range of 1-20 mW[18]. CW operation was also reported with two single mode CW CO_2 lasers. With input signal levels of 25 W at 10 μm wavelengths, an output power level just below 10^{-7}W was obtained at a frequency of ~3000 GHz[19]. Obviously, the output power at SMM wave would be even lower as a result of the dependence of output frequency.

To raise the output power, besides a higher input power, an

increase of optical nonlinearity and/or a decrease of the beam cross-section is required. Some recent studies of harmonic generation at metal and semiconductor surfaces and in thin film geometries suggests that an additional contribution to the nonlinearity could come from the electron plasmas present in the crystal[20,21]. Moreover, the use of thin film structures not only offers the desired reduction in beam cross-section but also leads in the direction of component integration at SMM wave frequencies.

It is thus in our interest to re-examine the process of difference frequency generation in planar structures. The canonical structure considered is given in Fig. 12a. It has five interspersed layers of dielectric and semiconductor materials. The semiconductor layers (the cross-hatched regions) may be intrinsic or doped GaAs material. Two laser waves, propagating collinearly in the $\hat{z}$-direction, are mainly confined within the center layer which, in the rest of this chapter, will be referred to as the optical waveguide. Due to the nonlinearity in the optical waveguide, MM or SMM waves are produced at the difference frequency. The propagation characteristic is determined by the dielectric property of the planar structure at that frequency.

In this work, special attention is paid to the optical nonlinearity, phase-matching condition and absorption effect and their dependence on electron plasma density existing in the

structure. In Section 3.1, we review the propagation characteristic of both the optical and SMM waves in the canonical structure. In Section 3.2, the origin of the optical nonlinearity in GaAs is discussed and the distribution of the induced polarization source is determined. In Section 3.3, general expressions for the output fields are derived using two alternate approaches. In Section 3.4, an explicit expression for the efficiency of power conversion is obtained for a sample structure which takes into consideration the phase-matching condition and the absorption effect. Finally, in Section 3.5, we assess qualitatively the effect of a biasing magnetic field on the various aspects of the difference frequency generation scheme.

3.1 Wave Propagation

3.1.1 Optical Wave Propagation

Consider the propagation of optical waves in the planar structure. In our model, the optical waveguide consists of a thin slab of GaAs sided by two thick layers of loss free dielectric material. At optical frequencies, the dielectric constant, ε_1, of the outer dielectric regions should have a much smaller value than that of the GaAs material so as to ensure a good confinement of the optical beams within the GaAs layer. On the other hand, it should have a value large enough so as to retard the MM wave sufficiently to meet the phase-matching condition. Quartz, which has a

dielectric constant of 4 has proven to be a good choice since it offers a compromise between the above two requirements. Also it has the additional advantage of a small loss tangent at both the optical and MM wave frequencies.

For the center GaAs layer, its dispersive and absorptive characteristics may be changed by introducing free carriers into the medium. However, at optical frequencies, these carrier-induced dispersion and absorption effects can be neglected if the plasma concentration is less than $10^{16}cm^{-3}$. Then, we have a dielectric waveguide with a thin slab of dielectric constant 10.8 sandwiched between two thick layers of lower dielectric constant materials. Optical wave propagation in such a structure is well understood and the analysis can be found in many texts[22]. Here we will state briefly the results. Let the wave propagation be along the $\hat{z}$-direction and the structure uniform in the y-direction. There exist two types of eigenmodes, TE and TM, which have nonzero field components E_y, H_x, H_z and H_y, E_x, E_z respectively. Because of the symmetry of the structure, the modes can be further decomposed into even and odd modes which have, respectively, a symmetric and asymmetric distribution of its transverse fields about the center plane. The dispersion equation and field distribution of the normal modes can be obtained from the general expressions given in Appendix I.1 by setting $t_1=t/2$ and $t_2=0$. A cutoff condition exists for the higher order modes. It is given by:

$$2\pi t(\varepsilon-\varepsilon_1)^{1/2} = n\lambda \qquad (3.1.2)$$

where

t = slab thickness

λ = free space wavelength

ε = dielectric constant of the slab

ε_1 = dielectric constant of the surrounding media

n = integer = order of mode

With λ~10.6 μm and a slab thickness of 2 μm, all higher order modes are below cutoff. Only the lowest order surface wave modes (TE_0, TM_0) can propagate at this frequency. In this work, the TE_0 mode is preferably chosen as the input mode because its fields are more closely confined within the slab.

3.1.2 MM and SMM Wave Propagatin

Now we determine the normal modes for the MM and SMM waves that propagate in the planar structure. First we have to realize that in this frequency range the dielectric property of the extrinsically doped n-type GaAs material depends strongly on the free electron concentration. For our canonical structure, the outer GaAs layers are moderately doped with electron plasma concentration around $2.1X10^{15}cm^{-3}$. The collision frequency is about 10^{11}Hz and is comparable to the MM wave frequency. The semiconducting material is in the plasma state. Its dielectric property is characterized by a dielectric 'constant' defined by:

$$\varepsilon(\omega) = \varepsilon^{(0)} - \omega_p^2/\omega^2 \qquad (3.1.3)$$

It is a function of both the plasma frequency and the frequency of the propagating wave. At MM wave frequencies, the presence of electron plasmas greatly reduce the dielectric constant. In fact, with $n_0 \simeq 10^{15} cm^{-3}$, the plasma frequency is in the THz, i.e., 10^{12} Hz, range. The doped GaAs region thus appears to have a negative dielectric constant.

The canonical model can be simplified further by neglecting the thin GaAs layer. The simplified structure is depicted in Fig. 12b. Generally, this waveguide structure can support two types of modes TE and TM. The symmetry of the structure enables the decomposition of the into even and odd modes. The dispersion characteristic and field distribution of each mode are again given by the equations in Appendix I.1. In the MM frequency range of interest, only the lowest order TE_0 and TM_0 modes can propagate without being cutoff. However, there is a major difference between the propagating optical wave modes and the MM wave modes. Because of the negative dielectric constant involved at the MM wave frequencies, the fields adhere to the interface instead of being confined within the n-GaAs region.

3.2 Induced Nonlinear Polarization

It is well known that a dielectric medium, when subject to an applied electric field $\underline{E}$, tends to become polarized due to the distortion of its internal charge distribution under the influence of the electric field. The resultant electric dipole moment per unit volume is called the electric polarization $\underline{P}$. In general, $\underline{P}$ is related to $\underline{E}$ through a field-dependent susceptibility tensor $\chi(\underline{E})$. In MKS units, this relationship is

$$\underline{P} = \varepsilon_0 \chi(\underline{E})\underline{E} \tag{3.2.1}$$

Expanding $\chi(\underline{E})$ as a power series in $\underline{E}$, eq. (3.2.1) may be rewritten as

$$\underline{P} = \varepsilon_0[\underline{\underline{\chi}}(\underline{E}) + \underline{\underline{\chi}}^{(2)}(\underline{E})\underline{E}]\underline{E} \tag{3.2.2}$$

where $\underline{\underline{\chi}}(\underline{E})$ is the linear susceptibility tensor and $\underline{\underline{\chi}}^{(2)}(\underline{E})$ is the quadratic nonlinear susceptibility tensor.

Similarly, when an EM wave is incident upon a medium, $\underline{P}$ will vary with the $\underline{E}$ component of the wave in accordance with eq. (3.2.2). The electric fields associated with ordinary monochromatic light sources are far too small for the observation of nonlinear phenomena. Therefore powerful optical lasers must be used. In the following two subsections, we will study the contributing nonlinear mechanisms of both the valence electrons and the electron plasmas. A quantitative estimation will be given to the nonlinear

polarization mechanism at the difference frequency by two laser waves.

3.2.1 Valence Electron Contribution

GaAs belongs to $\bar{4}3m$ crystal group. A medium with such a noncentrosymmetric crystal structure possesses nonlinear susceptibility of second and higher orders. Two waves of frequencies ω_1 and ω_2 will then interact nonlinearly in this medium. In the difference frequency generation case, the nonlinear polarization at the difference frequency $\Delta\omega = \omega_1 - \omega_2$ can be written in the form:

$$P_{v\alpha}^{NL}(\underline{r};\Delta\omega) = \Sigma_{\beta,\gamma}\varepsilon_0 \chi_{\alpha\beta\gamma}(\Delta\omega,\omega_1,\omega_2)E_\beta(\underline{r};\omega_1)E_\gamma^*(\underline{r};\omega_2) \tag{3.2.3}$$

Here $\underline{E}$ represents the total electric field of the propagating wave and α, β, γ refer to the crystal axes. The nonlinear susceptibility $\chi_{\alpha\beta\gamma}$ may depend on all three frequencies. The symbol v is used to indicate that the contribution comes from the valence electrons and the symbol * represents the complex conjugate.

In the MM and SMM wave range where the interaction between the EM fields and the optical phonons is negligible, the nonlinear susceptibility is no longer frequency dependent. It becomes[17](MKS units):

$$\chi_{\alpha\beta\gamma} = \begin{cases} \chi_v = 42.9 \times 10^{-12} \text{ m/V} & \alpha \neq \beta \neq \gamma \\ 0 & \text{otherwise} \end{cases} \qquad (3.2.4)$$

Clearly the valence electron contributions to the nonlinearity will depend on the relative orientation of the electric field with respect to the crystal axes.

Consider a GaAs waveguide geometry in which the surface normal $\hat{x}$ coincides with the crystal axis $\alpha(001)$ while the direction of propagation $\hat{z}$ makes an angle θ with the crystal axis $\gamma(010)$. Two optical waves of frequencies ω_1 and ω_2 propagating in such a structure will induce a nonlinear polarization distribution. At the difference frequency, the nonlinear polarization contributed by the valence electrons can be expressed in terms of its component in the waveguide coordinates (xyz), i.e.,

$$\begin{aligned}
&P_{vx}^{NL}(\Delta\omega) \\
&= \varepsilon_0 \chi_v \{ \sin 2\theta [E_z(\omega_1) E_z^*(\omega_2) - E_y(\omega_1) E_y^*(\omega_2)] \\
&\quad + \cos 2\theta [E_z(\omega_1) E_y^*(\omega_2) + E_y(\omega_1) E_z^*(\omega_2)] \} \\
&P_{vy}^{NL}(\Delta\omega) \\
&= \varepsilon_0 \chi_v \{ -\sin 2\theta [E_x(\omega_1) E_y^*(\omega_2) + E_y(\omega_1) E_x^*(\omega_2)] \\
&\quad + \cos 2\theta [E_x(\omega_1) E_z^*(\omega_2) + E_z(\omega_1) E_x^*(\omega_2)] \} \\
&P_{vz}^{NL}(\Delta\omega) \\
&= \varepsilon_0 \chi_v \{ \sin 2\theta [E_x(\omega_1) E_z^*(\omega_2) + E_z(\omega_1) E_x^*(\omega_2)] \\
&\quad + \cos 2\theta [E_x(\omega_1) E_y^*(\omega_2) + E_y(\omega_1) E_x^*(\omega_2)] \}
\end{aligned} \qquad (3.2.5)$$

If the crystal is cut in such a way that $\theta=45^{o}$, then nonlinear polarization induced by two TE_0 mode optical waves only one nonzero component, i.e., the transverse component P_{vx}^{NL}. is symmetrically distributed in the transverse plane of the opt waveguide. Thus it gives a net, first order contribution to nonlinearly generated wave.

3.2.2 Electron Plasma Contribution

The presence of electron plasmas may increase the nonli polarizability. As was indicated in eq. (2.2.1), the nonli effect comes in through the Lorentz force term and the convec derivative term. Other mechanisms that result in the second o effect in polarization may also exist. For example, the elec plasma concentration varies with the pump field intensity. satisfies the following continuity equation:

$$\partial n/\partial t = -\nabla\cdot(n\underline{v}) \qquad (3.2.$$

In the presence of the pump fields of frequencies ω_1 and ω_2 can Fourier expand all fields in the form:

$$\begin{aligned}&\underline{E}(\underline{r},t)\\ &= \underline{E}(\underline{r};\omega_1)e^{-j\omega_1 t} + \underline{E}(\underline{r};\omega_2)e^{-j\omega_2 t}\\ &+ \underline{E}(\underline{r};\omega_1+\omega_2)e^{-j(\omega_1+\omega_2)t} + \underline{E}(\underline{r};\omega_1-\omega_2)e^{-j(\omega_1-\omega_2)t}\\ &+ \cdots\cdots\cdots + c.c.\end{aligned}$$

$$
\begin{aligned}
&\underline{B}(\underline{r},t) \\
&= \underline{B}(\underline{r};\omega_1)e^{-j\omega_1 t} + \underline{B}(\underline{r};\omega_2)e^{-j\omega_2 t} \\
&+ \underline{B}(\underline{r};\omega_1+\omega_2)e^{-j(\omega_1+\omega_2)t} + \underline{B}(\underline{r};\omega_1-\omega_2)e^{-j(\omega_1-\omega_2)t} \\
&+ \ldots\ldots\ldots + \text{c.c.} \\
&\underline{v}(\underline{r},t) \\
&= \underline{v}(\underline{r};\omega_1)e^{-j\omega_1 t} + \underline{v}(\underline{r};\omega_2)e^{-j\omega_2 t} \\
&+ \underline{v}(\underline{r};\omega_1+\omega_2)e^{-j(\omega_1+\omega_2)t} + \underline{v}(\underline{r};\omega_1-\omega_2)e^{-j(\omega_1-\omega_2)t} \\
&+ \ldots\ldots\ldots + \text{c.c.} \\
&n(\underline{r},t) \\
&= n_0 + n(\underline{r};\omega_1)e^{-j\omega_1 t} + n(\underline{r};\omega_2)e^{-j\omega_2 t} \\
&+ n(\underline{r};\omega_1+\omega_2)e^{-j(\omega_1+\omega_2)t} + n(\underline{r};\omega_1-\omega_2)e^{-j(\omega_1-\omega_2)t} \\
&+ \ldots\ldots\ldots + \text{c.c.}
\end{aligned}
\qquad (3.2.7)
$$

where c.c. represents complex conjugate terms.

The only d.c. term included in these expressions is the n_o term which represents the steady state electron concentration. All the other d.c. terms are omitted since these give only higher order contributions to the polarization nonlinearity.

Under the small perturbation assumption, we can solve eqs. (1.2.1) and (3.2.6) by successive approximations. Substituting eq. (3.2.7) into the above equations and collecting the first order terms, we get

$$\underline{v}^{(1)}(\omega) = (je/m^*\omega)\underline{E}(\omega) \qquad (3.2.8)$$

Throughout the rest of the chapter, the spatial dependence of all the field related quantities is implied.

Collecting the second order term of difference frequency $\Delta\omega$, we get

$$\begin{aligned}&\underline{v}^{(2)}(\Delta\omega)\\&=\{\frac{je/m^*}{\Delta\omega}[\underline{E}(\Delta\omega)+\underline{v}^{(1)}(\omega_1)\times\underline{B}^*(\omega_2)]\\&+\frac{[\underline{v}^{(1)}(\omega_1)\cdot\nabla]\underline{v}^{(1)*}(\omega_2)}{(\Delta\omega)^2}\}+(1\leftrightarrow 2)^*\end{aligned}\tag{3.2.9}$$

In the above expression, $(1\leftrightarrow 2)^*$ means that similar terms can be obtained by the interchange of the roles of 1 and 2 followed by a conjugate operation.

Now we can derive the expression for the nonlinear current. At the difference frequency, the current induced by electron plasmas is given by:

$$\underline{J}(\Delta\omega)=-e(n_0\underline{v}^{(2)}(\Delta\omega)+n(\omega_1)\underline{v}^{(1)*}(\omega_2)+n(\omega_2)\underline{v}^{(1)}(\omega_1))\tag{3.2.10}$$

which consists of a linear part and a nonlinear part. If the frequencies of the input waves are much greater than the difference frequency, i.e., when $\omega_1, \omega_2 \gg \Delta\omega$, we get a simplified expression for the nonlinear current:

$$\underline{J}^{NL}(\Delta\omega) = \frac{j\varepsilon_0\omega_p{}^2 e/m^*}{\omega_1\omega_2}\left\{\frac{\nabla[\underline{E}(\omega_1)\cdot\underline{E}^*(\omega_2)]}{\Delta\omega}\right.$$
$$\left. + \frac{\omega_1\underline{E}(\omega_1)[\nabla\cdot\underline{E}^*(\omega_2)]+\omega_2\underline{E}^*(\omega_2)[\nabla\cdot\underline{E}(\omega_1)]}{\omega_1\omega_2}\right\} \qquad (3.2.11)$$

In this equation the last term on the right hand side is significant only at the boundary where the gradient of the electric field is large. In the present analysis, this surface current term is neglected and only the bulk current is taken into consideration.

Instead of using the bulk current, the nonlinear effect can also be expressed in terms of a nonlinear polarization. The bulk current expressed by eq. (3.2.11) is equivalent to a polarization term:

$$\underline{P}_c^{NL}(\Delta\omega) = \frac{-\varepsilon_0\omega_p{}^2 e/m^*}{\omega_1\omega_2(\Delta\omega)^2}\nabla[\underline{E}(\omega_1)\cdot\underline{E}^*(\omega_2)] \qquad (3.2.12)$$

where c refers to the conduction electron contribution. This is a general expression for the nonlinear polarization induced in the interior of a nonlinear medium by two pump fields. With two TE_0 modal waves as input, the nonlinear polarization induced through the presence of electron plasmas has two nonzero components, the transverse component P_{cx}^{NL} and the longitudinal component P_{cz}^{NL}, both of which are in phase with the polarization wave induced by the valence

electrons. However, for the transverse component, the plasma induced polarization does not add significantly to the total polarization wave. This is because the transverse component consists of the product of a symmetric transverse electric field component and an asymmetric longitudinal magnetic field component. So its distribution is always asymmetric which yields only the higher order effects. The plasma-induced longitudinal component, however, is always symmetrically distributed about the center plane. Thus it plays an important part in the polarization wave.

3.3 Surface Wave Generation

In this section, we determine the intensity and distribution of the EM field generated by a nonlinear polarization wave of phase factor $e^{j(\Delta\omega t - \Delta k_z z)}$. The most commonly used method is a plane wave approximation which assumes that both the input and output waves are uniform plane waves of infinite extent. However, this assumption is only applicable to waves propagating within a bulk crystal of large transverse dimensions. For the multilayered planar structure in which we are interested the boundary conditions must be taken into consideration and a more rigorous treatment is required.

The Green's function method can be used to calculate the generated field when boundaries are present. Bonsall and Maradudin[23] have reported the use of a Green's function formalism in the presence of a single-interface structure. Expressions derived

for the generated field contain a 'resonant' denominator which vanishes as the phase-matching condition is achieved. This implies that the generated field is 'resonantly enhanced' by the phase-matching condition. However, these results can only be obtained for a loss free structure and one which also provides an unlimited propagation length. The manifestation of the 'resonance enhancement effect' arises from the constructive interference along an 'infinitely long' interaction path. If either loss or finite length occurs then the results have to be modified.

In this work, a more realistic physical model is used. The structure is shown in Fig. 12a. It is symmetric about the x=0 plane and has a finite length L in the direction of wave propagation. Absorption effects may also be present.

The problem of difference frequency generation can be formulated as follows. At the difference frequency $\Delta\omega$, the macroscopic field generated via the induced polarization $\underline{P}^{NL}$ is described by Maxwell's equations:

$$\nabla X\underline{E} = -j\Delta\omega\mu_0\underline{H} \tag{3.3.1}$$

$$\nabla X\underline{H} = j\Delta\omega\underline{D} \tag{3.3.2}$$

where

$$\underline{D}(\underline{r};\Delta\omega) = \varepsilon_0\varepsilon(x;\Delta\omega)\underline{E}(\underline{r};\Delta\omega)+\underline{P}^{NL}(\underline{r};\Delta\omega) \tag{3.3.3}$$

$$\varepsilon(x;\Delta\omega) = \begin{cases} \varepsilon(\Delta\omega) & |x| \le t \\ \varepsilon_1 & t_1 \le |x| \le t_1 + t \\ \varepsilon_2(\Delta\omega) & t_1 + t \le |x| \le t_1 + t_2 + t \\ \varepsilon_3 & |x| \ge t_1 + t_2 + t \end{cases} \tag{3.3.4}$$

$$\underline{P}^{NL}(\underline{r};\Delta\omega) = \begin{cases} \underline{P}^{NL}(x)\, e^{j(\Delta\omega t - \Delta k_z z)} & |x| \le t \\ 0 & |x| > t \end{cases} \tag{3.3.5}$$

If the thickness of the center layer is small compared to the wavelength of the polarization wave and all the other transverse dimensions involved, the distribution of the nonlinear polarization can be approximated by a delta function centered at the x=0 plane. That is,

$$\underline{P}^{NL}(x) = \underline{P}^{NL}\,(x) \tag{3.3.6}$$

The center layer can then be eliminated from the analysis. The remaining problem is then to determine the amplitude and distribution of the field generated by a nonlinear polarization source for the simplified planar structure given in Fig. 12b. Two different methods can be used to achieve this end.

3.3.1 Green's Function Formalism

The Green's function formalism is widely used in determining the fields radiated by a given system of sources. The Green's function is the solution to a given differential equation, together with specified boundary conditions, with the source functions being of unit strength and localized at a point in space. Then the total radiated field can be obtained by multiplying the Green's function with the source strength and integrating over the source distribution. In other words, it converts a differential equation problem into an integration problem. In our case, we have, by combining eqs. (3.3.1)- (3.3.3), a differential equation:

$$\Sigma_\beta[\partial^2/\partial x_\alpha \partial x_\beta - \delta_{\alpha\beta}\nabla^2 - \delta_{\alpha\beta}k_0^2\varepsilon(x;\Delta\omega)]E_\beta(\underline{r};\Delta\omega) = (k_0^2/\varepsilon_0)P_\alpha^{NL}(\underline{r};\Delta\omega) \tag{3.3.7}$$

where $k_0=\Delta\omega/c$ and $E_\beta(\underline{r},\Delta\omega)$ is a component of the macroscopic electric field. This inhomogeneous partial differential equation can be converted into an integral equation:

$$E_\alpha(\underline{r};\Delta\omega) = E_\alpha^{(0)}(\underline{r};\Delta\omega) - \Sigma_\gamma(k_0^2/\varepsilon_0)\int G_{\alpha\gamma}(\Delta\omega|\underline{r},\underline{r}')P_\gamma^{NL}(\underline{r};\Delta\omega)d^3r' \tag{3.3.8}$$

where $G_{\alpha\gamma}$ ($\Delta\omega$ $|\underline{r},\underline{r}'$) is a Green's function which satisfies the equation:

$$\Sigma_\beta[\partial^2/\partial x_\alpha \partial x_\beta - \delta_{\alpha\beta}\nabla^2 - \delta_{\alpha\beta}k_0^2\varepsilon(x;\Delta\omega)]G_{\beta\gamma}(\Delta\omega|\underline{r},\underline{r}') = -\delta(\underline{r}-\underline{r}')\delta_{\alpha\gamma} \tag{3.3.9}$$

and $E_\alpha^{(0)}(\underline{r};\Delta\omega)$ is the solution for the corresponding homogeneous equation.

To proceed further, it is convenient to introduce the Fourier representation of $G_{\alpha\beta}(\Delta\omega|\underline{r},\underline{r}')$ and $\delta(\underline{r}-\underline{r}')$:

$$G_{\alpha\beta}(\Delta\omega|\underline{r},\underline{r}') = \int dk_z e^{-jk_z(z-z')} g_{\alpha\beta}(k_z\Delta\omega|x,x')/2\pi \quad (3.3.10)$$

and

$$\delta(\underline{r},\underline{r}') = \delta(x-x')\int dk_z e^{-jk_z(z-z')}/2\pi \quad (3.3.11)$$

The form of this representation reflects the fact that the system characterized by the dielectric constant $\varepsilon(x;\Delta\omega)$ (eq. (3.3.4)) is invariant in the y-z plane only. Substitution of eqs. (3.3.10), (3.3.11) into eq. (3.3.9) yields the following set of differential equations for the Fourier coefficient $g_{\alpha\beta}(k_z\Delta\omega|x,x')$:

$$\begin{bmatrix} \varepsilon(x;\Delta\omega)k_o^2-k_z^2 & 0 & jk_z\partial/\partial x \\ 0 & \varepsilon(x;\Delta\omega)k_o^2+\partial^2/\partial x^2-k_z^2 & 0 \\ jk_z\partial/\partial x & 0 & \varepsilon(x;\Delta\omega)k_o^2+\partial^2/\partial x^2 \end{bmatrix} \underline{\underline{g}}=\delta(x-x')\underline{\underline{I}} \quad (3.3.12)$$

The solution has to satisfy the appropriate boundary conditions at the interfaces as well as at $x=\pm\infty$.

The Fourier coefficient $g_{\alpha\beta}$ of the Green's functions can be obtained following reference (24). The unit source is considered to be localized at the x=0 plane. The only nonzero Fourier coefficients are g_{xx}, g_{yy}, g_{zz}, g_{xz} and g_{zx} which satisfy a set of differential equations given by eq. (3.3.12). Using the boundary conditions given by eqs. A22(a)-(f) in reference (24), we solve for these primary functions in a straight forward manner. The results are given in Appendix I.2.

Now let's examine these functions more carefully. Functions g_{xz} and g_{zz} have the same denominator

$$\begin{aligned} &DN1 \\ &=[1+(\varepsilon_2 k_3/\varepsilon_3 k_2)\tanh k_2 t_2)+(\varepsilon_1 k_2/\varepsilon_2 k_1)\tanh k_1 t_1[(\varepsilon_2 k_3/\varepsilon_3 k_2)-\tanh k_2 t_2] \\ &=0 \end{aligned} \qquad (3.3.13)$$

where

$$k_{1,2}^2 = k_0^2\varepsilon_{1,2}-k_z^2$$
$$k_3^2 = -k_0^2\varepsilon_3 + k_z^2$$

Both functions become bounded when the denominator vanishes. Similarly, function g_{zx} and g_{xx} become infinite when

$$\begin{aligned} &DN2 \\ &=[1+(\varepsilon_2 k_3/\varepsilon_3 k_2)\tanh k_2 t_2]\tanh k_1 t_1+(\varepsilon_1 k_2/\varepsilon_2 k_1)[\tanh k_2 t_2-(\varepsilon_2 k_3/\varepsilon_3 k_2)] \\ &=0 \end{aligned} \qquad (3.3.14)$$

and g_{yy} becomes infinite when

$$\begin{aligned} &DN3 \\ &=[1+(k_3/k_2)\tanh_2 t_2]\tanh_1 t_1+(k_2/k_1)(\tanh_2 t_2-k_3/k_2) \\ &=0 \end{aligned} \tag{3.3.15}$$

Comparing this with the dispersion equations given in Appendix I.1, we find that eqs. (3.3.13) and (3.3.14) correspond, respectively, to the dispersion equations of the odd and even TM surface wave modes of the planar structure under investigation. Similarly, the root of eq. (3.3.15) leads to the even-TE surface wave modes. Thus, the Fourier coefficient $g_{\alpha\beta}(k_z\Delta\omega|x,0)$ becomes singular when k_z approaches the propagation constant k_n of some surface wave mode.

Combining eqs. (3.3.8) and (3.3.10), we can now evaluate the components of the generated field. Taking advantage of the delta function distribution for $\underline{P}^{NL}$, the integral can be reduced to:

$$\begin{aligned} &E_\alpha(\underline{r};\Delta\omega) \\ &= -\Sigma_\beta(k_0^2/\varepsilon_0)P_{0\beta}^{NL}\int dk_z e^{j(\Delta\omega t-k_z z)} g_{\alpha\beta}(k_z\Delta\omega|x,0)\int dz' e^{j(k_z-\Delta k_z)z'}/2\pi \end{aligned} \tag{3.3.16}$$

If the structure is lossless and infinitely long in the direction of

wave propagation, as was obviously the case in ref. (23), then making use of the fact that

$$\int dz' e^{j(k_z-\Delta k_z)z'}/2\pi = \delta(k_z-\Delta k_z) \qquad (3.3.17)$$

we can carry out the integration quite easily. Each term of the summed series retains the same functional form as the corresponding Fourier coefficient $g_{\alpha\beta}(k_z\Delta\omega|x,0)$, except that the integration variable k_z is now replaced by the propagation constant Δk_z of the polarization wave. Consequently the amplitude of the generated field demonstrates the same singular behavior as $g_{\alpha\beta}$, i.e., it becomes infinitely large when Δk_z approaches the propagation constant k_n of the proper surface wave mode. This is the so-called phase-matching condition.

The above conclusion is true only if the interaction length is infinite and no damping effect is present. The violation of either condition will void the validity of eq. (3.3.17) and hence all the results that follow. Unfortunately, this is exactly what we can expect in the physical world. Therefore, the problem of EM wave generation in the presence of a planar waveguide structure has to be re-examined with the finite interaction length and/or losses being taken into consideration.

Again, eq. (3.3.16) can be used to evaluate the electric field generated by the nonlinear polarization source. However,

problem arises with the integration. Under the condition of a finite interaction length L, the integration over dz' no longer yields a delta function. Instead, we obtain a sinc function which has an argument $(k_z-\Delta k_z)L/2$. This function describes a spatial interference pattern which acquires a maximum value when k_z is made equal to Δk_z. In addition, if loss is present, all wave vectors become complex numbers and the expression for the interference pattern has to be modified accordingly[17].

The next step then is to integrate over dk_z. This takes into account the interference effect due to the source distribution in momentum space. The integrand now includes the Fourier coefficient $g_{\alpha\beta}$, the sinc function and some phase factors. Extra care must be taken in performing the integration because of the presence of singularity in the function $g_{\alpha\beta}$. The integral, as discussed in reference (25), can be decomposed into two parts, a branch-cut integral and the residues contributed by the enclosed poles. The branch-cut integral represents the radiation field with a continuous eigenvalue spectrum while the residues at the enclosed poles are the surface wave modes.

It has been noted previously that the function $g_{\alpha\beta}$ has poles at some k_z values which correspond to the propagation constant of some surface wave modes. For the planar structure under investigation, there exist four types of surface wave modes, i.e., even and odd TE

and TM modes. Generally, the excited surface wave is a linear superposition of all these modes. Now consider a special example in which the polarization source has only an x-component. Then in eq. (3.3.16), only the terms associated with g_{xx} and g_{zx} give nonzero results. This leads to the even-TM modal surface waves. The electric field of the m^{th} order surface wave modes can be obtained from eq. (3.3.16):

$$E_{\alpha}^{m} = (k_0^2/\varepsilon_0)2\pi j(\text{residue at } k_z=k_m) \tag{3.3.18}$$

Using the expression given in Appendix I.2 for $g_{\alpha\beta}$, we get the following explicit expressions for the electric field. In the i^{th} region, the electric field of the m^{th} order surface wave mode has components:

$$E_{xi}^{m}=-(jA/k_i^m)[(df_i^{(x)}/dx)|_{DN2=0,k_z=k_m}]/[(dDN2/dk_z)|_{k_z=k_m}] \tag{3.3.19}$$

$$E_{zi}^{m}=(Ak_i^m)[f_i^{(x)}|_{DN2=0,k_z=k_m}]/[(dDN2/dk_z)|_{k_z=k_m}] \tag{3.3.20}$$

where

$$A = Fk_m p_{ox}^{NL}/(2\varepsilon_0 k_1^m \varepsilon_i \cos k_1^m t_1 \cos k_2^m t_2)$$

Note that k_i^m represents the transverse wave numbers of the m^{th} order surface wave mode. Both expressions in eqs. (3.3.19) and (3.3.20) contain a factor F which is the product of a function

L sinc($(\Delta k_z - k_m)L/2$) and a phase factor $e^{j(\Delta\omega t - k_m z)}$. The s function is defined by sinc(x)=sin(x)/x where $x=(\Delta k_z - k_m)L/2$. It negligible magnitude for all the eigenvalues k_m except the one wh is in the vicinity of Δk_z. Thus the surface mode which meets t phase-matching condition becomes the dominant mode. And the fi strength of the generated wave is proportional to the interact length L.

Eqs. (3.3.19) and (3.3.20) represent the field distribut of an even-TM modal surface wave excited by the $\hat{x}$-component o nonlinear polarization source. Similarly, the $\hat{y}$ and $\hat{z}$-components a nonlinear polarization source excite only surface waves of even and odd-TM nature, respectively. When all three components present, only the mode which satisfies the phase-matching condit is excited.

3.3.2 Lorentz Reciprocity Theorem Approach

We may also adopt a different approach utilizing the Lore Reciprocity Theorem in calculating the generated fields. Lorentz Reciprocity Theorem is applied in a similar way to t illustrated in ref. (25). However, the polarization source is distributed along the direction of propagation as given by (3.3.6) and generates one or more surface wave modes and a radiat field. Since the various surface wave modes are orthogonal to another, as well as to the radiation field, the total radiated fi

may be represented as follows:

for the forward direction of propagation

$$\underline{E} = \Sigma_m a_m \underline{E}_m e^{j(\Delta\omega t - k_m z)} + \underline{E}_R^+ \qquad (3.3.21)$$

$$\underline{H} = \Sigma_m a_m \underline{H}_m e^{j(\Delta\omega t - k_m z)} + \underline{H}_R^+ \qquad (3.3.22)$$

for the reverse direction of propagation

$$\underline{E} = \Sigma_m b_m \underline{E}_m e^{-j(\Delta\omega t - k_m z)} + \underline{E}_R^- \qquad (3.3.23)$$

$$\underline{H} = \Sigma_m b_m \underline{H}_m e^{-j(\Delta\omega t - k_m z)} + \underline{H}_R^- \qquad (3.3.24)$$

where $\underline{E}_R$, $\underline{H}_R$ is the radiation field and $\underline{E}_m$, $\underline{H}_m$ the m^{th} surface wave mode field.

The total field is a solution of the equations

$$\nabla X \underline{E} = -j\Delta\omega\mu_0 \underline{H} \qquad (3.3.25)$$

$$\nabla X \underline{H} = j\Delta\omega(\varepsilon \underline{E} + \underline{P}^{NL}) \qquad (3.3.26)$$

while the surface wave mode is a solution of the source-free field equations. Let $\underline{E}$ and $\underline{H}$ be the total radiated field and $\underline{E}_m$, $\underline{H}_m$ the m^{th} surface wave mode field for the planar structure under investigation. If we choose a closed loop S on the x-z plane, consisting of two transverse paths at z_1 and z_2 and two longitudinal paths at infinity, then the 2-dimensional Lorentz Reciprocity Theorem gives:

$$\oint_S (\underline{E} \times \underline{H}_m - \underline{E}_m \times \underline{H}) \cdot \hat{n} d\ell = \iint j\Delta\omega \underline{P}^{NL} \cdot \underline{E}_m dA \qquad (3.3.27)$$

Following the same argument as was used in ref. (25), we arrived at these results for the amplitude of the radiated wave of the m^{th} mode:

in the forward direction of propagation,

$$a_m = - \frac{\iint \underline{E}_m e^{-j(\Delta\omega t - k_m z)} \cdot j\Delta\omega \underline{P}^{NL} dxdz}{\int \underline{e}_m \times \underline{h}_m \cdot \hat{z} dx}$$

$$= - \frac{\int \underline{E}_m(x=0) \cdot j\Delta\omega \underline{P}_0^{NL} e^{j(k_m - \Delta k_z)z} dz}{\int \underline{e}_m \times \underline{h}_m \cdot \hat{z} dx} \qquad (3.3.28)$$

in the reverse direction of propagation,

$$b_m = - \frac{\int \underline{E}_m(x=0) \cdot j\Delta\omega \underline{P}_0^{NL} e^{j(k_m + \Delta k_z)z} dz}{\int \underline{e}_m \times \underline{h}_m \cdot \hat{z} dx} \qquad (3.3.29)$$

where $\underline{e}_m$, $\underline{h}_m$ are transverse electric and magnetic field components associated with $\underline{E}_m$ and $\underline{H}_m$, respectively.

In order to show that this method yields the same result as that of the Green's function method, we again consider the special case of having only an $\hat{x}$-component for the nonlinear polarization source. The dot-product in the numerator of eqs. (3.3.28) and (3.3.29) suggests that the excited surface wave must have a nonzero E_x component at the x=0 plane. This condition is satisfied by the even-TM mode surface waves. For a structure of finite length L, the integration over dz again yields a sinc function which, in turn,

yields the phase-matching condition, i.e., $k_n=\Delta k_z$, for the n^{th} order surface wave mode. The amplitude of this phase-matched surface wave can then be obtained by substituting the proper expressions of $\underline{E}_n$ and $\underline{H}_n$ into the following equation:

$$a_n = \frac{j\Delta\omega P_{ox} e_{nx}(x=0)L}{2\int_{-\infty}^{\infty} e_{nx} h_{ny} dx} \tag{3.3.30}$$

where P_{ox} is the $\hat{x}$-component of $\underline{P}_o^{NL}$ obtained by performing an integration over dx on both sides of eq. (3.3.6). The electric field of the excited surface wave is then given by

$$\underline{E} = a_n \underline{E}_n e^{j(\Delta\omega t - \Delta k_z z)} \tag{3.3.31}$$

Note that for the even-TM mode, the electric field has only $\hat{x}$ and $\hat{z}$ components. And eq. (3.3.31) gives the same results as eqs. (3.3.19) and (3.3.20). These are the general expressions which are applicable to both the lossy and lossless conditions.

3.4 Power Conversion Efficiency

3.4.1 The Phase-Matching Condition

The importance of achieving phase-matched operation has been mentioned previously. In the difference frequency generation case, this requires the propagation constant (or phase velocity) of the output wave to be equal to that of the driving wave of the same frequency. Usually this will not happen for intrinsic GaAs

waveguide as it suffers from dispersion, i.e., the phase velocities differ for waves of different frequencies. The phase velocity of the driving wave is in general smaller than that of the driven wave. In Fig. 13 we show part of the dispersion curve of the input TE_0 mode optical waves from which the dispersion curve of the driving wave is constructed. The result is given in Fig. 14. Also shown are the dispersion curves for the driven MM waves. These are the normal modes of an intrinsic waveguide such as that shown in Fig. 12b, except that all the GaAs layers are intrinsic. In this frequency range of interest, only even TE_0 and TM_0 modal surface waves can propagate without cutoff. However, the dispersion curves of these even-mode driven waves always stay to the left of that of the driving wave. That is, its phase velocity is always larger than that of the driving wave. A phase-matching operation is possible only if the MM wave can be slowed down by some means.

Many ingeneous phase matching techniques were reported which used different ways to compensate for the dispersion effect. We are particularly interested in the magneto-optic phase-matching technique[26]. As we have seen previously, at MM or SMM frequencies, the dielectric property of GaAs material can be controlled through the plasma density. The plasma contribution to the dielectric constant is of opposite sign to the lattice contribution. The degree of compensation can be adjusted by varying either the plasma concentration or the applied magnetic field strength.

The application of a static magnetic field for phase-matching purpose will be discussed in Section 3.5. Here we check the feasibility of achieving phase-matched operation through the control of plasma concentration. It is illustrated by an example given in Fig. 15. For a plasma level of $\sim 2.1 \times 10^{15} cm^{-3}$, phase matching is obtained for the driving and driven waves at a frequency around 270 GHz where their dispersion curves intersect. A tuning range of $\sim$210 GHz can be obtained by varying the plasma density by $\sim$50%. Both optical and electronic means have been reported[27,28] for the dynamic control of the plasma concentration.

3.4.2 Absorption Effect

The major hinderance in obtaining high efficiency in power conversion, besides the phase mismatch, is the absorption effect in the waveguide structure. There are two major mechanisms, the dielectric loss and the free carrier loss, that cause attenuation in the nonlinear generation process. The dielectric loss is attributed to the multiphonon processes in the GaAs layers and the intervening quartz layers. In the low temperature operation, this loss mechanism can be neglected for both the optical and MM waves when compared with the free carrier absorption mechanism.

Free carrier absorption occurs when the semiconducting material is extrinsically doped. In an n-type GaAs medium, electrons lose energy when impeded by impurity ions. This scattering process is

characterized by a momentum relaxation time or collision time which is related to the electron mobility by $\tau = e\mu/m^*$. It is well known that the electron mobility in semiconductor material decreases as the doping level increases. Therefore, a high impurity concentration will increase the collision frequency and thus the loss. For the input optical waves, this absorption effect is still negligible if the plasma frequency is much lower than the optical wave frequencies. This happens when the plasma concentration is less than $10^{16}cm^{-3}$. For the output MM waves, however, the presence of an electron plasma brings an appreciable amount of attenuation. The collision frequency is comparable to the frequency of the changing field in spite of the low doping level ($\sim 10^{15}cm^{-3}$) and low ambient temperature ($77^{o}K$).

Clearly, the consideration of phase-matched operation and low free carrier absorption presents two oppositing restraints on the plasma concentration. The phase-matching operation demands the slowing down of the MM waves which is achieved by introducing electron plasmas into the guiding medium. However, since the electron plasmas are accompanied by the presence of impurity ions, considerable loss arises.

The only way to curtail the loss while at the same time maintain a phase-matched operation is to generate the electron plasmas by some means other than extrinsic doping. Thus, the

electron mobility will be maintained at a near-intrinsic value ($\sim 2X10^5 cm^2/V\text{-}sec$) and the momentum relaxation time can be as high as $20X10^{-12}s$. In Fig. 15, we find the attenuation range from about 1.5 to 3.5 dB/mm for frequencies between 160 to 380 GHz. If extrinsic doping is used, the electron mobility will retain only half of its intrinsic value and the attenuation per unit length will be at least doubled.

3.4.3 Sample Calculation

Now we will quantatively estimate the efficiency of power conversion for the proposed thin film structure. The efficiency of the difference frequency generation by nonlinearly mixing two optical waves is given by:

$$e(\Delta\omega) = \frac{S(\Delta\omega)}{S(\omega_1)+S(\omega_2)} \qquad (3.4.1)$$

where S stands for the net energy flux per unit width of the wave in the transverse direction. At optical frequencies, the time-averaged Poynting vector of a TE-mode wave travelling in the $\hat{z}$-direction is given by:

$$\langle \underline{S}(x;\omega) \rangle = Re(\underline{E} X \underline{H}^*)/2 \qquad (3.4.2)$$

where $\underline{E}$ and $\underline{H}$ are the electric and magnetic fields.

The net input energy flux S per unit width is therefore

obtained:

$$S(\omega_{1,2}) = \int_{-\infty}^{\infty} \langle \underline{S}(x;\omega_{1,2}) \rangle \cdot \hat{z}\, dx$$

$$= t\left[\frac{1}{2t}\int_{-\infty}^{\infty} \frac{k_z(\omega_{1,2})}{\omega_{1,2}\varepsilon_0 \varepsilon(x;\omega_{1,2})} |\phi(x;\omega_{1,2})|^2 dx\right] |I_{1,2}|^2$$

$$= t\, T_{1,2} |I_{1,2}|^2 \qquad (3.4.3)$$

In the above expression t gives the thickness of the optical waveguide and $\varepsilon(x;\omega_{1,2})$ and $\phi(x;\omega_{1,2})$, defined by eqs. (3.3.4) and (I.1.4), respectively, describe the dielectric and field distributions. The term $T_{1,2}$ can be obtained from a knowledge of the field distribution at the respective frequency. $I_{1,2}$ gives a measure of the field strength. The total power of the input wave is then given by

$$P_{1,2} = ht T_{1,2} |I_{1,2}|^2 \qquad (3.4.4)$$

where h is the height of the structure.

The next task is to determine the energy flux of the generated output wave. At the difference frequency, the general expression for the energy flux per unit width associated with an excited n^{th} order surface wave mode is given by:

$$S(\Delta\omega) = |a_n|^2 \int_{-\infty}^{\infty} \underline{e}_n \times \underline{h}_n^* \cdot \hat{z}\, dx/2 \qquad (3.4.5)$$

where $\underline{e}_n$ and $\underline{h}_n$ represent the electric and magnetic field distribution and a_n measures the amplitude of the excitation. Among

all the excited surface wave modes, only the A branch of the even TM modes meets the phase-matching requirement. Therefore, energy transfers from the input waves into the A type MM wave mode. The excitation strength and energy flux can be obtained by substituting the proper expressions of the field distribution of mode A into eqs. (3.3.30) and (3.4.5), respectively. The results are:

$$a_e = \frac{-jP_{ox}\Delta\omega\,(E_{x1}|_{x=0})}{2\int_{-\infty}^{\infty}E_x(x)H_y^*(x)dx} \tag{3.4.6}$$

and

$$\begin{aligned} S(\Delta\omega) &= |a_e|^2\int_{-\infty}^{\infty}E_x(x)H_y^*(x)dx/2 \\ &= |a_e|^2\left[\int_0^{t_1}E_{x1}H_{y1}^*dx+\int_{t_1}^{t_1+t_2}E_{x2}H_{y2}^*dx+\int_{t_1+t_2}^{\infty}E_{x3}H_{y3}^*dx\right] \end{aligned} \tag{3.4.7}$$

where $\{E_{xi},\ H_{xi}\}$, $i=1,3$ can be obtained from eqs. (2.1.7)-(2.1.12)) by replacing the thicknesses T and W with t_1 and t_2, respectively. Note that the strength of the excitation, a_e, is linearly proportional to $\Delta\omega$. That is, the smaller the difference frequency, the weaker the excitation. It is also linearly proportional to P_{ox} which is obtained by integrating P_x^{NL}, the $\hat{x}$-component of the nonlinear polarization distribution, over dx, keeping in the integrand only the contribution from the valence electrons. Thus,

$$P_x = \frac{-\varepsilon_0\chi_v k_z(\omega_1)k_z(\omega_2)}{\omega_1\omega_2\varepsilon_0^2\varepsilon(x;\omega_1)\varepsilon(x;\omega_2)}\phi(x;\omega_1)\phi(x;\omega_2) \tag{3.4.8}$$

$$P_{ox} = 2\int_0^t P_x dx = tT_p I_1 I_2^* \qquad (3.4.9)$$

Clearly, P_{ox} depends on the amplitudes of both input waves. And its dependence on the source distribution is summed up in the term T_p.

Now we can calculate the energy flux per unit width of the output wave. By substituting eqs. (3.4.6) and (3.4.9) into eq. (3.4.7), we get the following expression:

$$S(\Delta\omega) = T_p^2 t^2 |I_1 I_2|^2 T_3 [\mathrm{sinc}((\Delta k_z - \beta_A)L/2)]^2 L^2 \qquad (3.4.10)$$

where β_A is the propagation constant of the excited mode A and T_3 is proportional to $(\Delta\omega)^2$. Under phase-matching operation and with no loss, the maximum efficiency of power conversion is obtained:

$$e(\Delta\omega) = \frac{tT_p^2 |I_1 I_2|^2 T_3 L^2}{(T_1 |I_1|^2 + T_2 |I_2|^2)} \qquad (3.4.11)$$

It is quadratically proportional to the difference frequency. For MM and SMM wave generation, the conversion efficiency usually is quite low. For example, if we take L=h=5λ=6.3 mm, two CO_2 lasers of output at 100 W each would generate a single-mode output wave at $\Delta f \sim 250$ GHz with power in the 10^{-8} W range. This is of the same order of magnitude as the power generated in a bulk crystal which has a cross section of 1 mmX6.3 mm and a length of 6.3 mm. Ideally,

a much longer structure could be used which will boost the efficiency quadratically as the length of the interaction path. However, in practical cases, the free carrier loss has to be included. All wave numbers will then assume complex values and the sinc function in eq. (3.3.10) has to be modified accordingly. Similar to eq. (2.29) of ref. (17), we also find an exponential term which severely shortens the effective interaction length. This is the major drawback of the use of solid state plasmas in the nonlinear generation process.

3.5 Magnetic Field Effect

We will devote the final section to discuss qualitatively the role of a d.c. magnetic field in nonlinear generation schemes. In the presence of the d.c. magnetic field, the doped GaAs medium becomes gyroelectric and its dielectric property is characterized by an asymmetric permittivity tensor. At a moderate magnetic field strength, e.g., B_0=3.8 KG, the cyclotron frequency is of the order of 10^{12} Hz which is much smaller than the optical frequency. Thus, the propagation characteristic of optical waves is not affected by the applied magnetic field. However, for the nonlinearly generated difference frequency wave, the frequency falls in the same range as ω_c. Therefore, cyclotron resonance may play an important role in the nonlinear generation process. Indeed, as was pointed out in references (29) and (30), the static magnetic field may have an important supportive role in the nonlinear benavior of the

conduction electrons.

Consider a d.c. magnetic field applied in the $\hat{y}$-direction transverse to the direction of wave propagation $\hat{z}$. Following the procedure given in Section 3.2.1, yet adding a d.c. term, i.e., $\underline{B}_0$, to eq. (3.2.6), we obtain the following expression for the nonlinear polarization induced by two TE_0 mode optical waves:

$$\underline{P}_c^{NL}(\Delta\omega) = \frac{-\varepsilon_0 \omega_p^2 e/m^*}{\omega_1 \omega_2 \Delta\omega((\Delta\omega)^2-\omega_c^2)} \{(\Delta\omega - j\omega_c \hat{y}X)[\nabla(\underline{E}(\omega_1)\cdot\underline{E}^*(\omega_2))]\} \tag{3.5.1}$$

In the above expression, the symbol X represents a vector cross-product operation. Clearly, the above equation shows a strong dependence on the applied magnetic field. It exhibits resonance phenomena as the cyclotron frequency approaches the difference frequency. In addition, the presence of the magnetic field causes the coupling between the longitudinal and transverse electric field components which may result in an increase in the nonlinear polarizability. We will not exploit the resonance phenomenon here since in this study the magnetic field strength is predetermined by the phase-matching condition which, as will be seen later, requires that $\omega_c \approx \Delta\omega/3$. The coupling of the longitudinal and transverse components, however, may prove to be important in the generation process.

For two input optical waves of TE_0 mode, eq. (3.5.1) yields two nonzero components. Comparing with eq. (3.2.12), we find that the presence of a d.c. magnetic field brings an additional term to the transverse component of the nonlinear polarization source P_{cx}^{NL}. This term is proportional to the applied magnetic field. It is in phase with the contribution from the valence electrons and, more important, it has a symmetric distribution inside the optical waveguide. Therefore, the electron plasmas now contribute significantly in the nonlinear generation process. Similarly, the presence of the magnetic field may also introduce an extra term into the longitudinal nonlinear polarization component. However, the induced polarization has an asymmetric distribution inside the waveguide and gives only a higher order contribution to the generated field.

Now we would like to find the amplitude and distribution of the MM wave generated by the nonlinear polarization in the presence of a static magnetic field. We again use the models shown in Figs. 12a and 12b. The magnetic field can be applied to the structure in two ways. In the first case, a static magnetic field in the $\hat{y}$-direction is applied uniformly across the whole structure. At the difference frequency, the induced polarization has two nonzero components, both of which are symmetrically distributed inside the optical waveguide. The transverse component consists of contributions from both the valence electrons and the conduction electrons while the

longitudinal component is induced solely by the conducti electrons. In the second case, the d.c. magnetic field stays in a assumes opposite directions in the two thick n-GaAs layers and static magnetic field exists in the thin GaAs region. Therefor the conduction electrons only contribute to the longitudin component of the nonlinear polarization while the valence electro are the sole contributor to the transverse polarization componen For the generated MM wave, the presence of a static magnetic fie in the outer n-GaAs layers changes these regions into anisotrop media. Thus the analysis given in Section 3.3 on the surface wa generation has to be modified.

We will first study the dispersion characteristic and fie distribution of the normal mode MM waves in the presence magnetoplasmas. The next task is to determine the intensity a mode structure for the output waves. Here we do not intend perform an exact analysis using dyadic Green's function or t modified Lorentz Reciprocity Theorem on anisotropic substrate Rather, we will only characterize the output wave qualitativel The output wave mode determination will be based on the followi two criteria. First, the excited wave must have a nonzero electr field component along the direction of the polarization sourc Secondly, the phase velocity of the output wave must match with th of the driving wave.

In the presence of a d.c. magnetic field, the dispersion characteristic of the normal modes can be obtained from the following transcendental equation:

$$e^{-2k_2T_2}\,\frac{e^{2k_2T_2}(R_1e^{2k_1T_1}-R_2e^{-2k_2T_2})-(R_3e^{2k_1T_1}-R_4e^{-2k_1T_1})}{e^{2k_2T_2}(R_5e^{2k_1T_1}-R_6e^{-2k_1T_1})-(R_7e^{2k_1T_1}-R_8e^{-2k_1T_1})} \qquad (3.5.2)$$

where

$$k_{1,3}^2 = -\gamma^2-k_0^2\varepsilon_{1,3}$$
$$k_2^2 = -\gamma^2-k_0^2\varepsilon_e$$

The coefficients R_1 to R_8 are obtained from the function

$$\begin{aligned}R(u,k,v,l,m,n,p,q) = {} & (k_2+uj\gamma\eta_4/\xi+k\varepsilon_e k_3/\varepsilon_3)\\ & \cdot(k_2+vj\gamma\eta_4/\xi+l\varepsilon_e k_1/\varepsilon_1)\\ & \cdot(k_2+mj\gamma\eta_2/\xi+n\varepsilon_e k_1/\varepsilon_1)\\ & \cdot(k_2+pj\gamma\eta_2/\xi+q\varepsilon_e k_3/\varepsilon_3)\end{aligned}$$

in the following way:

$$\begin{aligned}R_i &= R(\ u\ \ k\ \ v\ \ l\ \ m\ \ n\ \ p\ \ q)\\ R_1 &= R(-1\ \ 1\ \ 1\ \ 1\ -1\ \ 1\ \ 1\ \ 1)\\ R_2 &= R(-1\ \ 1\ \ 1\ -1\ -1\ -1\ \ 1\ \ 1)\\ R_3 &= R(\ 1\ -1\ -1\ -1\ -1\ \ 1\ \ 1\ \ 1)\\ R_4 &= R(\ 1\ -1\ -1\ \ 1\ -1\ -1\ \ 1\ \ 1)\\ R_5 &= R(-1\ \ 1\ \ 1\ \ 1\ \ 1\ -1\ -1\ -1)\end{aligned}$$

$$R_6 = R(-1 \quad 1 \quad 1 \quad -1 \quad 1 \quad 1 \quad -1 \quad -1)$$

$$R_7 = R(\ 1 \quad -1 \quad -1 \quad -1 \quad 1 \quad -1 \quad -1 \quad -1)$$

$$R_8 = R(\ 1 \quad -1 \quad -1 \quad 1 \quad 1 \quad 1 \quad -1 \quad -1)$$

where ξ and $\eta_{2,4}$ are defined by eqs. (1.2.4) and (1.2.6), with 2,4 referring to each of the two outer GaAs slabs. If the magnetic field is applied uniformly through the structure, we have $\eta_2=\eta_4$ in eq. (3.5.2). The waveguide modes can be decomposed into pure TE and TM modes and the propagation is reciprocal. The field distributions, however, are neither symmetric or anti-symmetric about the center plane because the structure is no longer symmetric electrically. The symmetry can be retained only if the d.c. magnetic field assume opposite directions in the two outer GaAs regions. Then in eq. (3.5.2), $\eta_2=-\eta_4$ and the normal modes are identical with those obtained for the two types of half structures each consisting of half of the original structure and an electric or magnetic wall at the x=0 plane. If an electric wall is in place, the structure becomes an insulated image guide. Its TE and TM modes have the same dispersison characteristic and field distribution as the odd TE and even-TM modes of the original structure. Similarly, if a magnetic wall is in place, the normal mode of the half structure correspond to the even TE and odd TM modes of the original structure.

According to Lorentz Reciprocity Theorem, a polarization source

will excite only those waves of which the electric field has nonzero component along the direction of the source vector. This is still true from the modified Reciprocity Theorem on anisotropic structures[31]. Consequently, no TE mode surface wave will be excited since its electric field is perpendicular to the polarization source. The output wave is thus pure TM in nature.

Now let's consider the case in which the d.c. magnetic field assumes opposite directions in the two thick GaAs layers. The dispersion curve of the odd TM modal surface waves has two branches, S and A, for both directions of propagation. However, surface waves can only propagate at frequencies above some cutoff value. Throughout the frequency range of interest, waves of an odd TM nature only exist as evanescent waves. The dispersion characteristic of the even TM normal modes in the MM and SMM wave range of interest is given in Fig. 16. A positive (negative) d.c. magnetic field strength indicates the forward (reverse) direction of propagation and a zero magnetic field strength represents an isotropic case. As was discussed in Section 2.1.1, there are, generally, two dispersion branches for both directions of propagation. However, the S branch wave is only weakly guided by the GaAs region. Its dispersion curve lies close to the light line which is far removed from the dispersion curve of the driving wave. Therefore, the phase-match requirement cannot be satisfied. The dispersion curve of the A branch, however, moves away from the light

line toward high dielectric light lines. This is a slow wave mode. Through proper control of the strength of the biasing magnetic field, this branch may be tuned to meet the desired phase-matching condition. From Fig. 16 we find that, without the static magnetic field, phase matching occurs at a frequency around 270 GHz. With a moderate magnetic field (B_0=1.9 KG) applied parallel to either $+\hat{y}$ or $-\hat{y}$ direction, a phase-matched operation can be maintained over a bandwidth of ~140 GHz.

Typical field distributions of the even-TM mode surface waves of the canonical structure are illustrated in Figs. 17a and 17b for both the forward and reverse directions of propagation. Note that the electric field has a tangential component which vanishes at the center plane. Consequently, there is no coupling between the tangential components of the electric field and the polarization source. On the contrary, there is a strong coupling between the normal components of the electric field and the polarization source. Therefore, the output wave is excited by the normal component of the polarization source induced through the valence electrons.

If the d.c. magnetic field is applied uniformly across the structure, the TM modal waves no longer exhibit the same properties as in the previous case. As shown in Fig. 18, the wave propagation is reciprocal and the dispersion curve of the normal modes generally consists of four branches: A_e, S_e and A_o, S_o. The subscripts e and

o are used to indicate the correspondence between these modes and the even and odd-TM modes of an electrically symmetric dielectric waveguide structure. Figure 19 shows the typical field distribution of the A_e mode of the canonical structure. The longitudinal field component no longer vanishes at the center plane. Therefore we can expect a coupling between this electric field component and the longitudinal component of the polarization wave induced through the electron plasmas. This brings an increase in the output power of the generated field due to the additional nonlinearity from the conduction electrons. However, this gain in power is at the expense of the bandwidth over which the phase matching operation is maintained. Comparing Figs. 16 and 18, we find the bandwidth is greatly reduced as a result of the external field.

More research work has to be done to understand fully and take advantage of the important role of solid state plasmas in the nonlinear generation process. The resonance phenomenon exhibited in the nonlinear behavior of magnetoplasmas may prove to be essential in overcoming the difficulty imposed on the nonlinear generation scheme by the free carrier absorption effect.

4. Conclusion

We have exploited the feasibility of utilizing solid state plasmas for potential MM and SMM applications, in particular, the non-reciprocal components and frequency conversion. In the first part of this work, the propagation characteristics of magnetoplasmons on one-dimensional insulated image guide structures and two-dimensional H-guide structures were investigated. Both showed strong non-reciprocity which were used as a basis for the design of non-reciprocal devices such as isolators and differential phase shifters. Optimization of device performance was applied on the insulated image guide structures. Sample calculations showed quite acceptable device behavior. The isolators were estimated to give an isolation ratio of 10:1 and an insertion loss of less than 0.5 dB/mm over a bandwidth of 65 GHz in the 400 GHz range. For differential phase shifters, phase shifts of 35°/mm to 65°/mm while the insertion loss of less than 1 dB/mm could be obtained over a bandwidth of ~90 GHz centered at 550 GHz. These highly promising results are expected to encourage further experimental and theoretical work in this direction to validate the predictions based on the current model and to develop models for more sophisticated device designs.

In the second part of this work, we examined the process of difference frequency generation of MM and SMM waves in planar

structures containing GaAs material. Special attention was paid to the optical nonlinearity, phase-matching condition and absorption effect and their dependence on the electron plasma density existing in the structure. The presence of electronic plasmas in GaAs layers enabled the necessary phase matching. However, it might also increase the attenuation, thus reduce the power conversion efficiency, through the free carrier absorption effect. Another limiting factor for the conversion efficiency is its quadratic dependence on the output frequency. Thus for MM and SMM waves which have frequencies far below the optical frequencies, the conversion efficiency stays low. A biasing magnetic field, however, may be used to overcome these difficulties. It was found that the presence of a d.c. magnetic field caused a coupling between the longitudinal and transverse electric field components which, in turn, resulted in an net increase in the nonlinear polarization induced through the presence of plasmas. Furthermore, magnetized plasmas also exhibited resonance phenomenon in its nonlinear behavior which may prove to be essential in obtaining a favored output.

More research work is needed for a quantitative evaluation of the nonlinear generation on anisotropic substrates containing solid state plasmas. This work takes the first step forward in that direction.

I. Appendices

I.1 Normal Modes of a Symmetric Dielectric Waveguide

For the planar waveguide structure shown in Fig. 12b, there exist four fundamental modes: even-TM, odd-TM, even-TE and odd-TE modes. Each mode is a solution of the dispersion equation:

$$Y_2(Y_{1b}-Y_2\tanh k_2 t_2)+Y_a(Y_2+Y_{1b}\tanh k_2 t_2)=0 \qquad (I.1.1)$$

where $k_{1,2,3}^2 = \omega^2\mu_0\varepsilon_0\varepsilon_{1,2,3} - \gamma^2$ and the Y's are defined as follows:

	even-TM	odd-TM	even-TE	odd-TE
$Y_{1,2}$	$\varepsilon_{1,2}/k_{1,2}$	$\varepsilon_{1,2}/k_{1,2}$	$k_{1,2}$	$k_{1,2}$
Y_a	$-\varepsilon_3/k_3$	$-k_3$	$-k_3$	$-k_3$
Y_{1b}	$Y_1/\tan k_1 t_1$	$-Y_1\tan k_1 t_1$	$-Y_1\tan k_1 t_1$	$Y_1/\tan k_1 t_1$

In the i^{th} region the field distribution can be found as follows:

TM-mode

$$E_{xi} = k_z\phi_i^{(e)}(x)/(\omega\varepsilon_o\varepsilon_i)$$

$$E_{zi} = (d\phi_i^{(e)}(x)/dx)/(j\omega\varepsilon_o\varepsilon_i) \qquad (I.1.2)$$

$$H_{yi} = \phi_i^{(e)}(x)$$

TE-mode

$$E_{yi} = -\phi_i^{(h)}(x)$$
$$H_{xi} = k_z \phi_i^{(h)}(x)/\omega\mu_o \qquad \text{(I.1.3)}$$
$$H_{zi} = (d\phi_i^{(h)}(x)/dx)/(j\omega\mu_o)$$

where

$$\phi_1(x) = \begin{cases} (1+b \tan k_2 t_2)\cos k_2 t_2 \cos k_1 x/\cos k_1 t_1 & \text{for even mode} \\ (1+b \tan k_2 t_2)\cos k_2 t_2 \sin k_1 |x|/\sin k_1 t_1 & \text{for odd mode} \end{cases}$$

$$\phi_2(x) = \cos k_2(|x|-t_1-t_2)-b \sin k_2(|x|-t_1-t_2)$$
$$\phi_3(x) = e^{-k_3(|x|-t_1-t_2)} \qquad \text{(I.1.4)}$$

and

$$b = \begin{cases} \varepsilon_2 k_3/\varepsilon_3 k_2 & \text{for TM mode} \\ k_3/k_2 & \text{for TE mode} \end{cases}$$

I.2 Fourier Coefficient of the Green's Functions

Listed below are the Fourier coefficients of the Green's functions for a structure depicted in Fig. 12b. The unit polarization source is located at the x=0 plane and the structure is uniform in the $\hat{y}$-direction. In the i^{th} region,

$$
\begin{aligned}
g_{zz}^{(i)} &= k_i f_i(x)/(2k_0^2\varepsilon_i \cos k_1 t_1 \cos k_2 t_2 \, DN1) \\
g_{xz}^{(i)} &= -(jk_z/k_i^2)(dg_{zz}^{(i)}/dx) \\
g_{zx}^{(i)} &= (jk_z DN1/k_1 DN2) g_{zz}^{(i)} \\
g_{xx}^{(i)} &= (\delta(x) - jk_z dg_{zx}^{(i)}/dx)/k_i^2 \\
g_{yy}^{(i)} &= h_i(x)/(2k_1 \cos k_1 t_1 \cos k_2 t_2 \, DN3)
\end{aligned}
\qquad \text{(I.2.1)}
$$

where

$$
\begin{aligned}
DN1 &= (1+bT_2) + (\varepsilon_1 k_2/\varepsilon_2 k_1) T_1 (b - T_2) \\
DN2 &= (1+bT_2) + (\varepsilon_1 k_2/\varepsilon_2 k_1)(T_2 - b) \\
DN3 &= (1+BT_2) T_1 + (k_2/k_1)(T_2 - B) \\
b &= \varepsilon_2 k_3/\varepsilon_3 k_2 \qquad B = k_3/k_2 \\
T_1 &= \tan k_1 t_1 \qquad T_2 = \tan k_2 t_2
\end{aligned}
$$

and

$$f_1(x)=[DN1\cosk_1t_1\cosk_1(x-t_1)-(1+bT_2)\cosk_1x]\cosk_2t_2/\sink_1t_1$$

$$=[-DN2\cos-_1t_1\cosk_1(x-t_1)+(1+bT_2)\sink_1x]\cosk_2t_2/\cosk_1t_1 \qquad (I.2.2)$$

$$f_2(x)=\sink_2(x-t_1-t_2)+b\cos-_2(x-t_1-t_2) \qquad (I.2.3)$$

$$f_3(x)=e^{-k_3}(x-t_1-t_2) \qquad (I.2.4)$$

$$h_1(x)=[DN3\cosk_1t_1\sink_1(x-t_1-t_2)+(1+BT_2)\cosk_1x]\cosk_2t_2/\cosk_1t_1 \qquad (I.2.5)$$

$$h_2(x)=\cosk_2(x-t_1-t_2)-B\sink_2(x-t_1-t_2) \qquad (I.2.6)$$

$$h_3(x)=e^{-k_3}(x-t_1-t_2) \qquad (I.2.7)$$

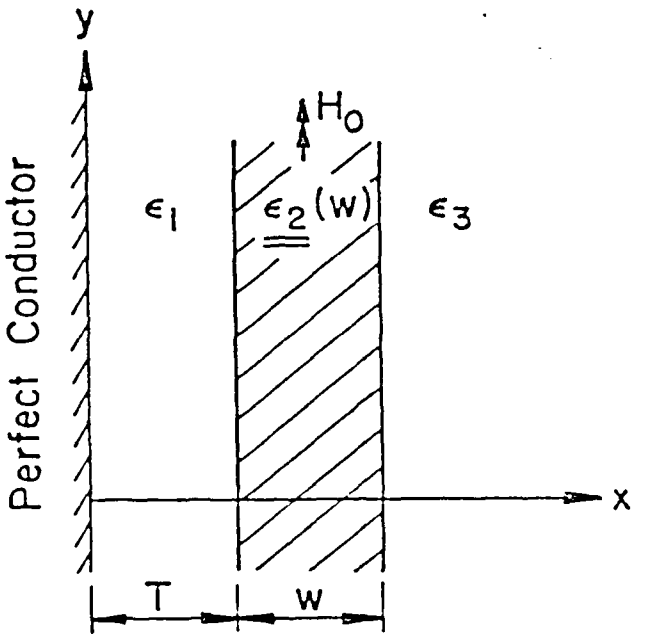

Figure 1. Insulated image guide structure.

4. Guiding and Control of MM-Waves by Surface Plasmons - Experimental Feasibility

In this section we review some of the feasibility estimates and experimental attempts which have been made to appraise the possibilities of using surface plasma waves in semiconductors to guide MM-waves in a practical environment. We consider here the case where no external magnetic fields are present and where the emphasis is on the simplest structure formed by a single planar dielectric interface. There are, however, serious difficulties with diagnostic evaluation of these concepts because of present problems of finding suitably flexibile MM-wave sources with the semiconductor structures of interest. While our laboratory work so far has yielded useful information about practical design considerations and material parameters for surface plasmon waveguides, we have not yet been successful with a definitive demonstration of an unambiguous propagation experiment. Nevertheless, with continuing advances in MM-wave source technology, future experiments should be possible with increasing versatility.

4.1 Semiconductor Material Considerations

A primary materials consideration in a practical surface plasmon MM-wave device concerns the need for low insertion losses. This implies a requirement for a low loss semiconductor and a suitable geometry for efficient coupling (excitation) of the plasma wave in a given structure.

The attenuation losses at MM-wave plasma frequencies in an elemental or a compound semiconductor are most likely to be dominated by free carrier absorption, i.e. from a finite electron or hole

AD-A143 767 APPLICATION OF SURFACE MAGNETOPLASMONS ON SEMICONDUCTOR 2/2
SUBSTRATES(U) BROWN UNIV PROVIDENCE RI
D M BOLLE ET AL. 31 DEC 83 ARO-17344.1-EL
UNCLASSIFIED DAAG29-80-K-0074 F/G 20/12 NL

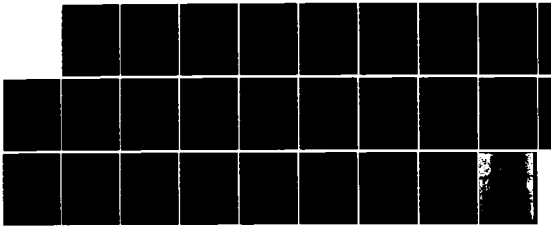

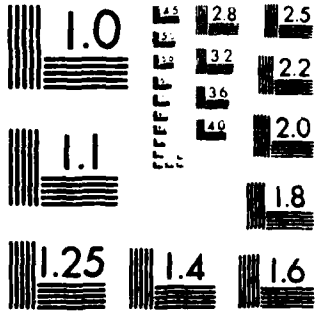

With recent advances in epitaxial materials growth there are now several attractive candidates to consider. Within the simple Drude model for the dielectric response function of an electron gas, we are mainly interested in finding and maintaining a long carrier scattering time. At the same time, a small effective mass is important in giving the large dispersive contribution necessary for a reasonable plasmon frequency at a moderate carrier density. In compound semiconductors such as GaAs, InSb, CdTe, or HgCdTe, the optical mode lattice vibrations have a polar component and this sets a practicable temperature limit to a surface plasmon device. This follows from the dominance of electron scattering by the polar mode scattering, typically at temperatures exceeding 77K in a material of low impurity concentration (for example, in InSb, the polar mode limited mobility at 77K is approximately 10^4).

In the absence of a significant phonon component, impurity scatterming will play the limiting practical role in the development of low loss surface plasmon guided wave structures. Here we are generally forced to make an optimum compromise between an impurity concentration high enough to yield the necessary carrier density but yet low enough to maintain the highest possible mobility. For example, the theoretically calculated impurity scattering limited maximum mobility in GaAs containing 10^{15} singly ionized impurities per cm^3 at 77K is slightly less than 10^6 $cm^2/Vsec$ (based on a Brooks-Herring formulation). This implies a mean scattering time of 4×10^{-11} sec for a carrier gas at the lattice temperature. The precise free carrier absorption losses will, of course, depend on the ratio of the plasmon frequency of the

carrier gas to that of the MM-wave (through the spatial extent to which the electric field of the MM-wave extends into the semiconductor) (3). A rough estimate for the attenuation of the surface wave intensity for a simple mode along the interface can be made through

$$L^{-1} \equiv 2\mathrm{Im}(\alpha) \simeq \frac{2\pi}{\lambda} \cdot \frac{\varepsilon_s'' \ (\varepsilon_0)^{3/2}}{\left(\varepsilon_s'^2 + \varepsilon_s''^2\right)} \tag{4.1}$$

where ε_s' and ε_s'' are the real and imaginary parts of the dielectric constant. The (free carrier) absorption coefficient is related to ε_s'' through $\alpha = 4\pi\varepsilon_s''/2n\lambda$, as usual.

Thus we may define a crude figure of merit for the case of a single dielectric interface by comparing the ratios of real and imaginary parts between different semiconductors. With the advances made recently in high quality growth of epitaxial GaAs, the theoretical limits of impurity scattering have been nearly achieved. Moreover, there have been significant developments in the area of MM-wave integrated devices based on this semiconductor. Thus, while the calculated figure of merit e.g. for InSb is somewhat higher, it would appear that GaAs continues to be the primary material in the near future for planned surface plasma wave guides.

Recently it has been shown that ultrahigh electron mobilities in GaAs can be reached in specific thin film structures of GaAs, grown by molecular beam epitaxy (32). The idea here is to utilize properties of semiconductor heterojunctions to facilitate spatial separation of electrons from their parent impurities. In this way the participation of impurity scattering has been significantly reduced in the so-called

inversion layers in GaAs/$Ga_{1-X}Al_xAs$ junctions. Consequently, low temperature mobilities up to 2×10^6 cm^2/Vsec have been achieved within a high density electron gas of bulk equivalent density exceeding 10^{19} cm^{-3}. For purposes of MM-wave surface plasma propagation such structures need to be modified to allow a larger spatial extent of the impurity ion-free region. Typically, at (the rather long) MM-wavelengths one is looking for plasma dimensions transverse to propagating direction on the order of 10 micrometers. Therefore, the possible exploitation of modulation doping techniques would require a multilayer structure where a larger effective plasma volume would be generated by a multi-quantum well composite of, say, several hundred layers thick. A somewhat different approach toward high mobility structures has been realized in the so-called nipi structure in which space charge fields between n-i-p type junctions cause periodic spatial modulation of the conduction and valence band extrema (33). This leads to electron and hole separation in local potential minima. In connection with the MM-wave surface plasma waveguide, the nipi structure may offer another attractive alternative in a multilayer configuration which might be integrable directly with future GaAs MM-wave sources and detectors.

4.2 Excitation from an External Source

We have made some initial attempts to examine surface plasma wave characteristics in the laboratory by using far infrared lasers for their excitation. This approach was chosen because of the unavailability (to us) of suitable solid state sources. We have encountered a number of difficulties in developing an unambiguous experiment in which verification of the propagation of an intrinsic surface wave could be

made. The primary problem has been to distinguish between a true surface wave and radiation which is simply scattered along the surface in the forward direction from the input coupling optics. These problems, which are discussed below, are not fundamentally prohibitive, but can be solved with an appropriately sophisticated laboratory approach.

The main source of MM-wave radiation in our work has been a continuous wave far-infrared laser, operating at the (SMM) wavelength of 496 micrometers. The active medium is $CH_3 3$ gas whose vibrational-rotational degrees of freedom are excited by a pump CO_2 laser. The FIR laser was constructed according to conventional design and consists of a length stabilized resonator with a hole output coupler. Electronic feedback was employed in the system to lock the emission of the CO_2 laser to a position of maximum absorption in CH_3 within the gain profile of the appropriate line of the laser. Similarly, active feedback (based on acousto-optic detection) controlled the resonator length and output power of the FIR laser. The spatial characteristics of the FIR laser were determined in part by the dielectric waveguide properties of the gas containing quartz tube and were of a mixture of EH-modes. As a consequence, the spatial characteristics of the output were generally not uniform in the transverse direction. This led to difficulties in coupling the laser output to the surface plasma waves in the semiconductor structure, typically situated within 10 to 30 cm outside the laser.

To excite and detect the surface plasma wave, we set up a prism coupling scheme similar to that used earlier at much higher frequencies to demonstrate the characteristics of surface plasmons in metals at visible wavelengths. (Another common alternative, the 'grating

coupling technique', was not attempted by us here.) The basic idea is to provide access to the semiconductor plasma which ordinarily would efficiently reflect radiation at frequencies below the bulk plasma frequency. A schematic arrangement is shown in Figure 14 where a prism of a sufficiently high index of refraction positioned above the semiconductor surface has the role of providing the appropriately reduced phase velocity in the direction parallel to the interface. In this scheme ('ATR' for attenuated total internal reflection) a small airgap is used as a spacer layer between the prism and the semiconductor surface. The coupling from the prism to the semiconductor plasma medium takes place across this gap whose thickness is usually a fraction of the wavelength in question. For a fixed incident frequency one now varies the angle of incidence and looks for a well-defined minimum in the reflectance from the prism structure as a signature of plasma wave excitation. Analytically, we can derive the following expression for the reflection coefficient for TH polarization in the ATR regime (the subscripts i, a, and p refer to the semiconductor plasma medium, the airgap, and the prism, respectively):

$$R_{TH} = \frac{1 + 2\exp(2ik_{zi}d)\mathrm{Re}[r^{*}_{PG}(\varepsilon_a k_{zi} - \varepsilon_i k_{za})/(\varepsilon_a k_{zi} + \varepsilon_i k_{za})]}{1 + 2\exp(2ik_{zi}d)\mathrm{Re}[r_{PG}(\varepsilon_a k_{zi} - \varepsilon_i k_{za})/(\varepsilon_a k_{zi} + \varepsilon_i k_{za})]} \qquad (4.2)$$

where d is the size of the airgap and the complex quantity r_{PG} is defined as

$$r_{PG} = \frac{\varepsilon_i k_{zp} - n_p^2 k_{zi}}{\varepsilon_i k_{zp} + n_p^2 k_{zi}} \quad , \qquad (4.3)$$

and the wavevector quantity k_{zp} by

$$k_{zp} = \left(n_p^2 \frac{\omega^2}{c^2} - k^2 \right)^{1/2} , \qquad (4.4)$$

where for the incident angle a at the prism base $k = n_p w/(c \sin a)$. The wavevector components k_{zi} and k_{za} are obtained from the dispersion relations

$$k_{zi} = \pm (\varepsilon_i \omega^2/c^2 - k^2)^{1/2}; \; k_{za} = \pm (\varepsilon_a \omega^2/c^2 - k^2)^{1/2} . \qquad (4.5)$$

This set of equations gives the necessary input for the choice of experimental geometry and we have used a microcomputer to calculate the solutions for a number of different materials as the semiconductor and the prism.

In conjunction with the CH_{3F} 496 micron source, we constructed an arrangement in which n-InSb was used as the plasma wave medium and germanium as the prism material. High quality bulk InSb is commercially available with a range of doping densities in the range of interest. For our initial purposes, InSb was considered an acceptable substitute for the generally more desirable GaAs because of cost, laboratory cutting and polishing, etc. The choice of Ge was made because of its high index of refraction and availability as high resitivity material. Two equilateral prisms were fabricated to facilitate input and output coupling, respectively. The detection of FIR radiation was made with a GaAs Schottky barrier diode or a pyroelectric bolometer and standard lock-in techniques. The airgap between the prism and the polished InSb surface was chosen to be in the range

of 50 to 100 microns. To verify the action of the prism as an input coupler, the reflection coefficient was measured for each prism for InSb at room temperature. A distinct dip was seen in the reflectance R(a) over a narrow range of values for the external angle of incidence a with respect to the prism side. The amplitude of the dip was usually rather small, however.

In order to study the propagation characteristics of a surface plasma wave in InSb, the two 3 mm wide prisms were mounted with spacers on the flat surface of a polished wafer of InSb, with a variable separation between them typically adjusted to about 1 cm. The entire arrangement was then mounted into the coldfinger of a liquid nitrogen cooled dewar at a nominal temperature. (The cooling is necessary to reduce the attenuation by phonon assisted free carrier absorption, as discussed above.) The FIR laser radiation was focussed onto the input coupling prism with a TPF lens. From this point on, however, serious difficulties were encountered in attempts to make unambiguous observations of the plasma wave propagation. Invariably, signals with a reasonable noise ration were detected off the output coupler but it was unclear whether they were originating from true surface modes or whether they represented FIR radiation which was simply diffracted into grazing along the surface. The origin of these ambiguities was determined to be our laser source whose spatial beam profile was quite nonoptimal for these purposes. (The problem of spatial non-uniformity of waveguide FIR lasers is a well-known drawback of these otherwise relatively simple devices.) A good deal of effort was expended in attempts to influence selectively what should have been

a proper surface mode signal, but with little success. For example, placing a beam block on the InSb surface strongly attenuated the output signals. Since a sizable fraction of the surface plasma wave field was calculated to extend into air, however, such a check did not yield a clear result.

From these initial experimental attempts it is clear that much care needs to be exercised in the design of a proper diagnostic and evaluative experimental program to demonstrate the feasibility of practical surface plasma MM or SMM-wave guiding. Much consideration needs to be given to a versatile (preferably frequency tunable) spatially well collimated and coherent source whose output can be directed into the chosen structure with small angular uncertainty. The air/semiconductor interface which we chose to examine may not be the best choice for a waveguide either (although it is certainly the simplest). A slab geometry could offer an advantage in permitting the input and output couplers to reside on the opposite sides of the semiconductor wafer. Finally, with the emergence of multilayer epitaxial structures it may be well worthwhile to consider the location of the surface active medium as a 'buried' layer. The coupling of the desired MM-wave signals may then be possible by e.g. grating techniques where the corrugation itself would be buried at or near the suitable interface.

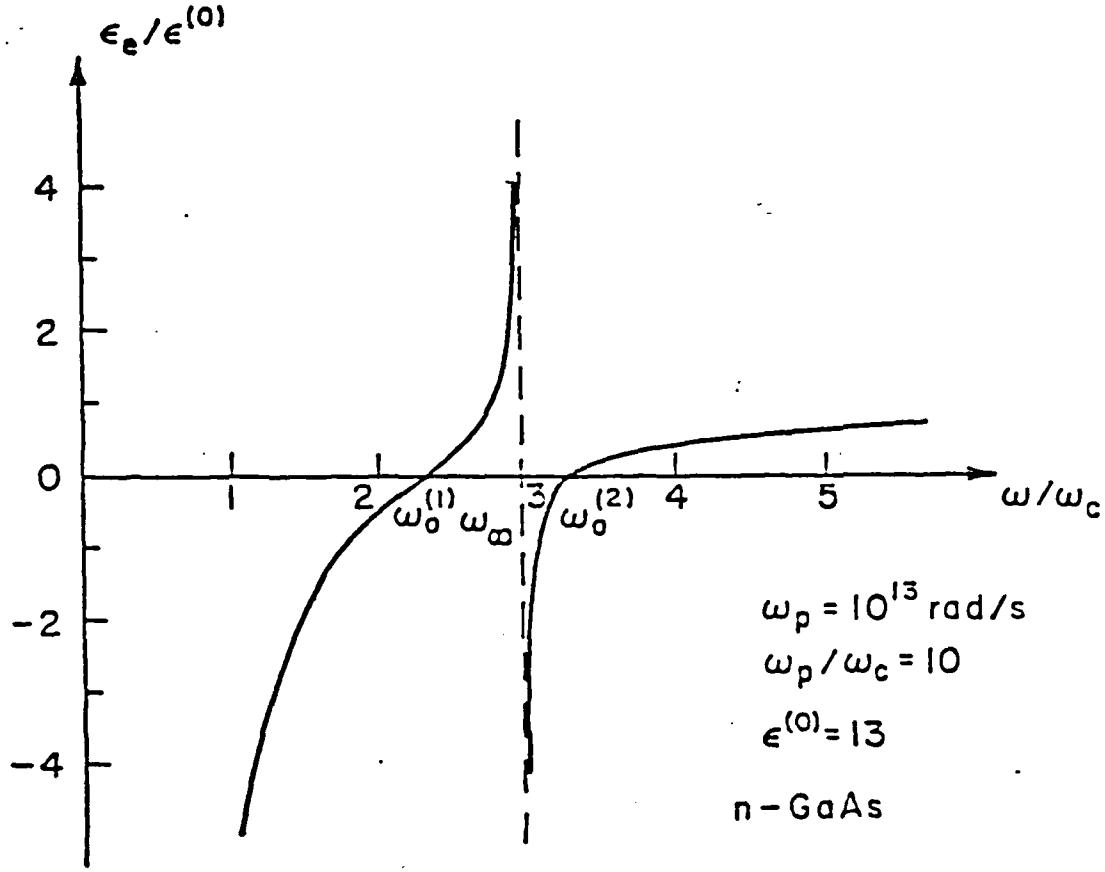

Figure 2.
Effective dielectric constant for anisotropic n-GaAs with d.c. magnetic field perpendicular to the propagation direction.

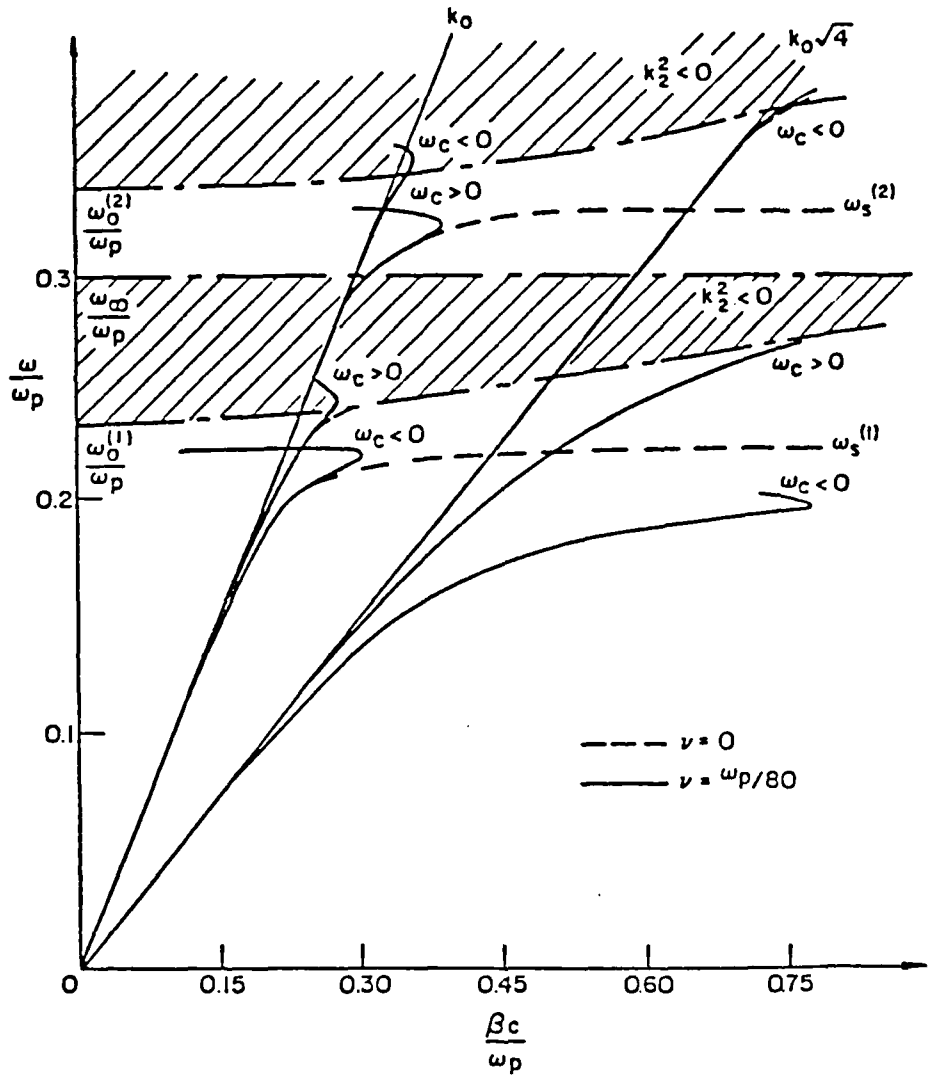

Figure 3. Dispersion curves for the lowest order single air-GaAs interface and single dielectric-GaAs interface. Long-dashed lines define radiation regions where $k_2^2 < 0$.

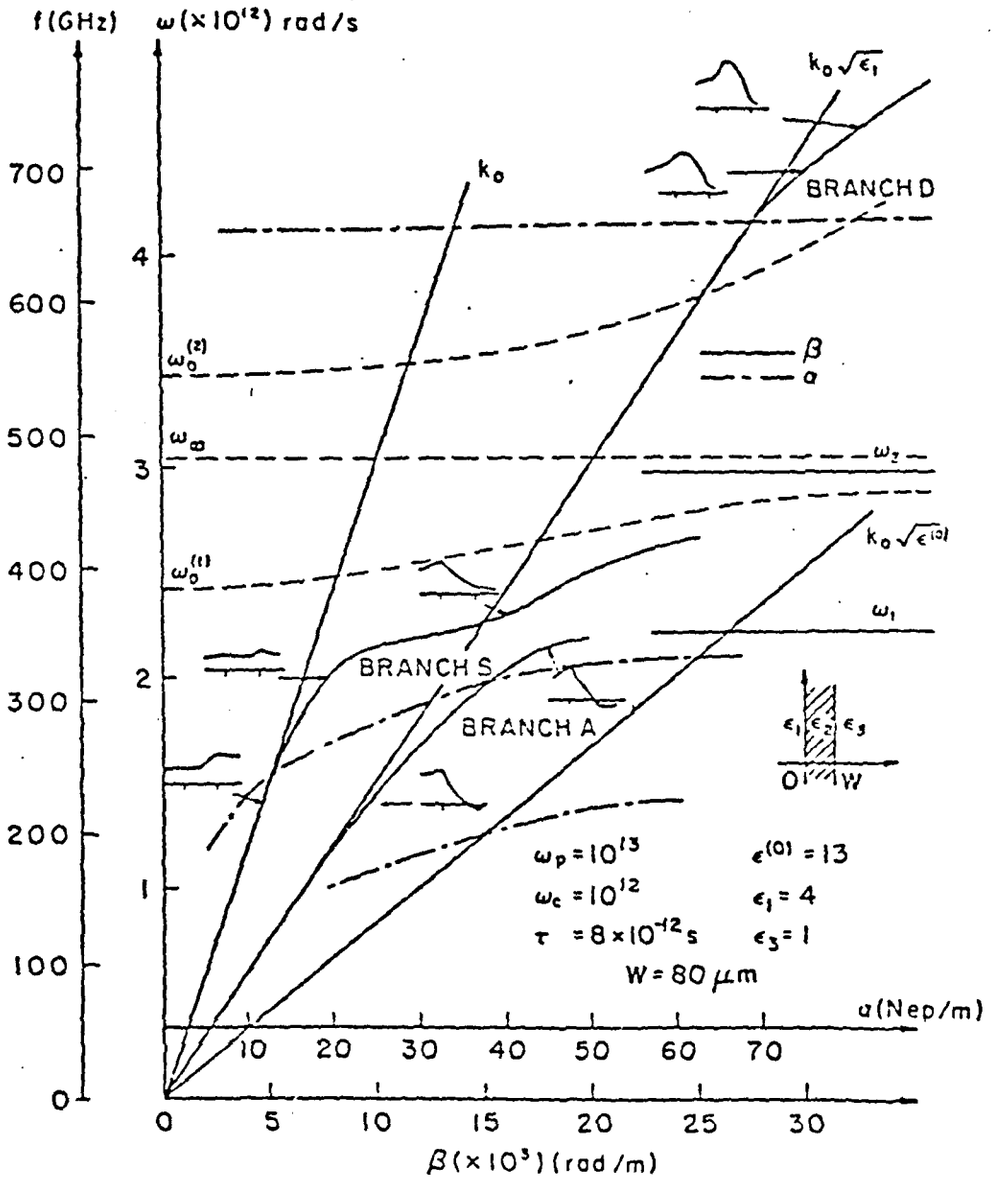

Figure 4a. Loss and dispersion diagram for the n-GaAs slab guide. Forward direction of propagation.

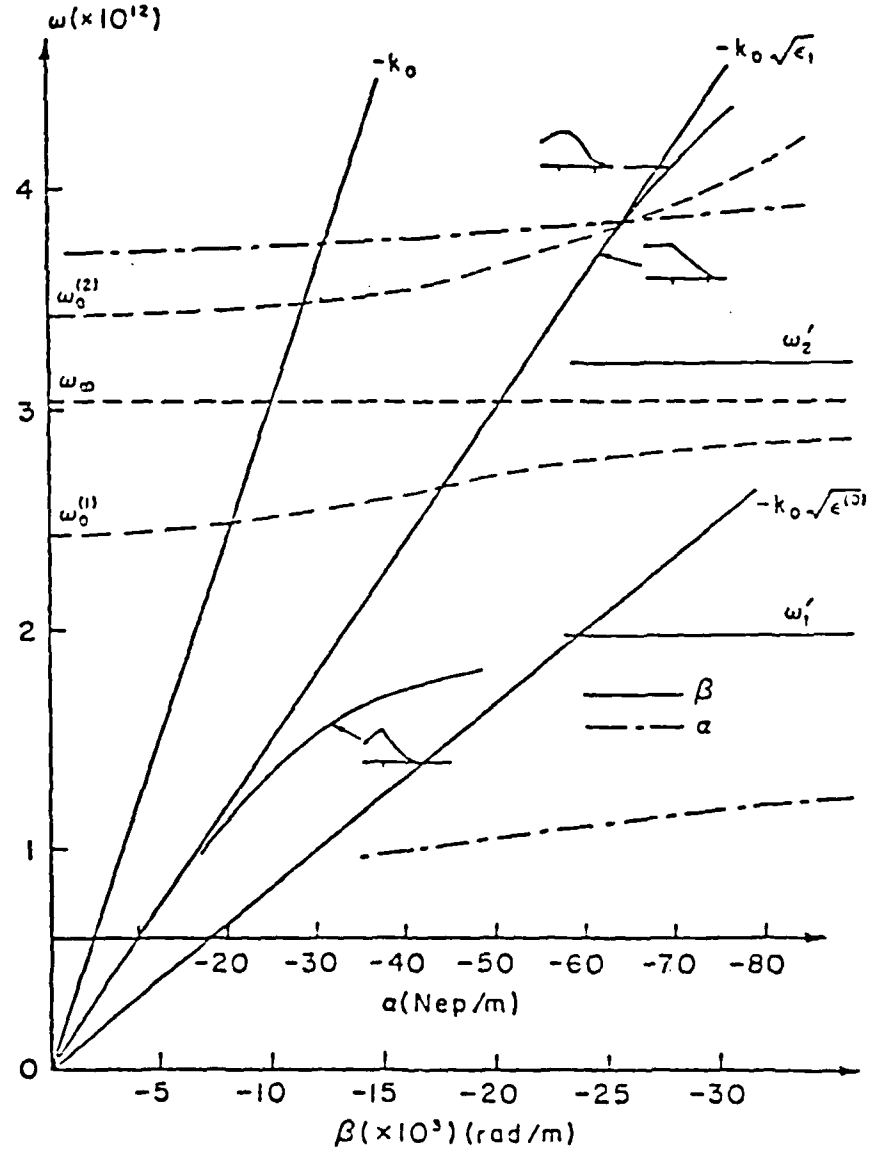

Figure 4b. Same as for Figure 4a. Reverse direction of propagation.

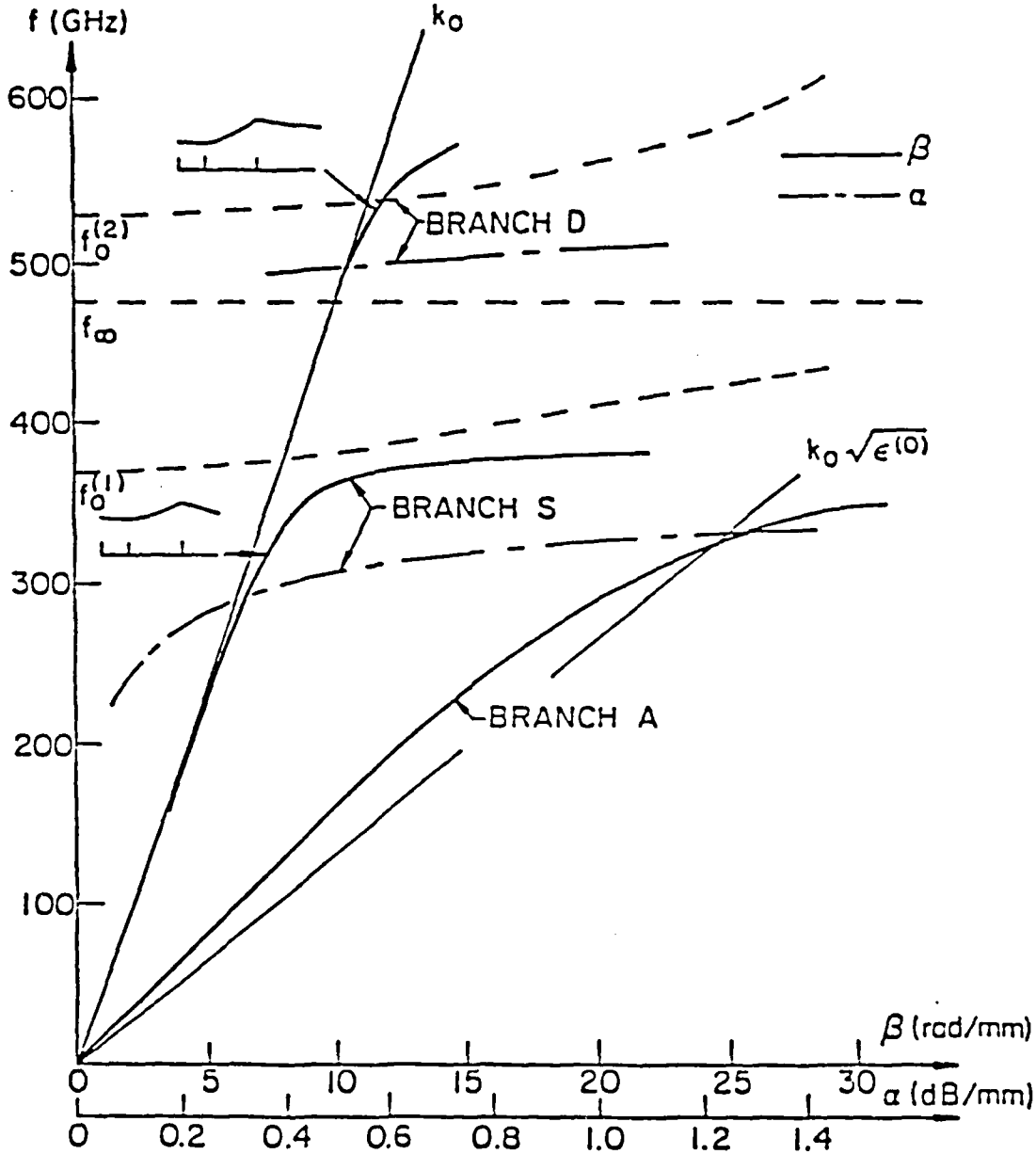

Figure 5a.
Dispersion diagram for insulated image guide structures with $\omega_p = 10^{13}$/s, $\omega_c = 10^{12}$/s, $\tau = 8 \times 10^{-12}$s, $\epsilon(0) = 13$, $\epsilon_1 = 4$, $\epsilon_3 = 1$, T = 25um and W = 50um. Forward direction of propagation.

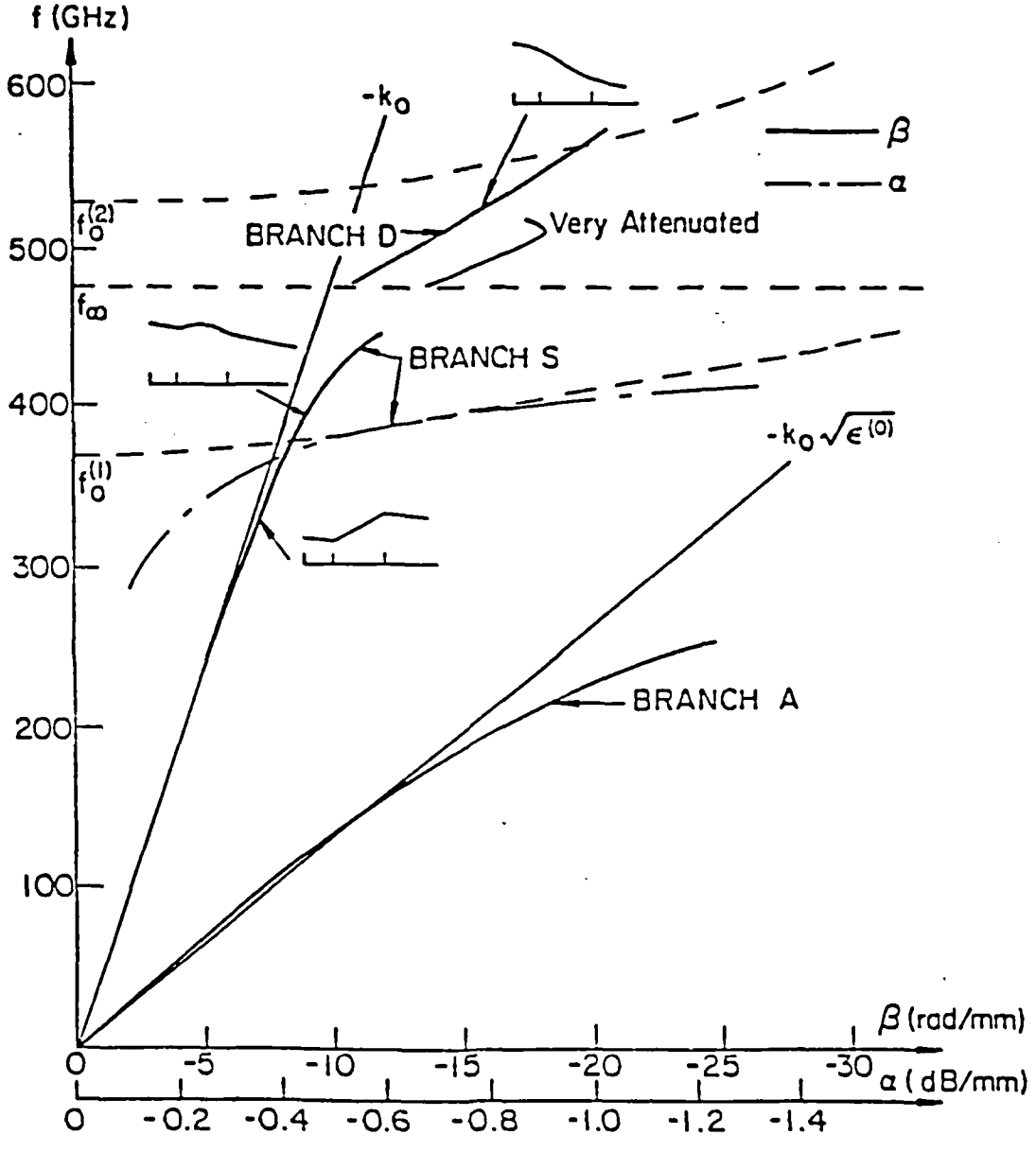

Figure 5b. Same case as for Figure 5a.
Reverse direction of propagation.

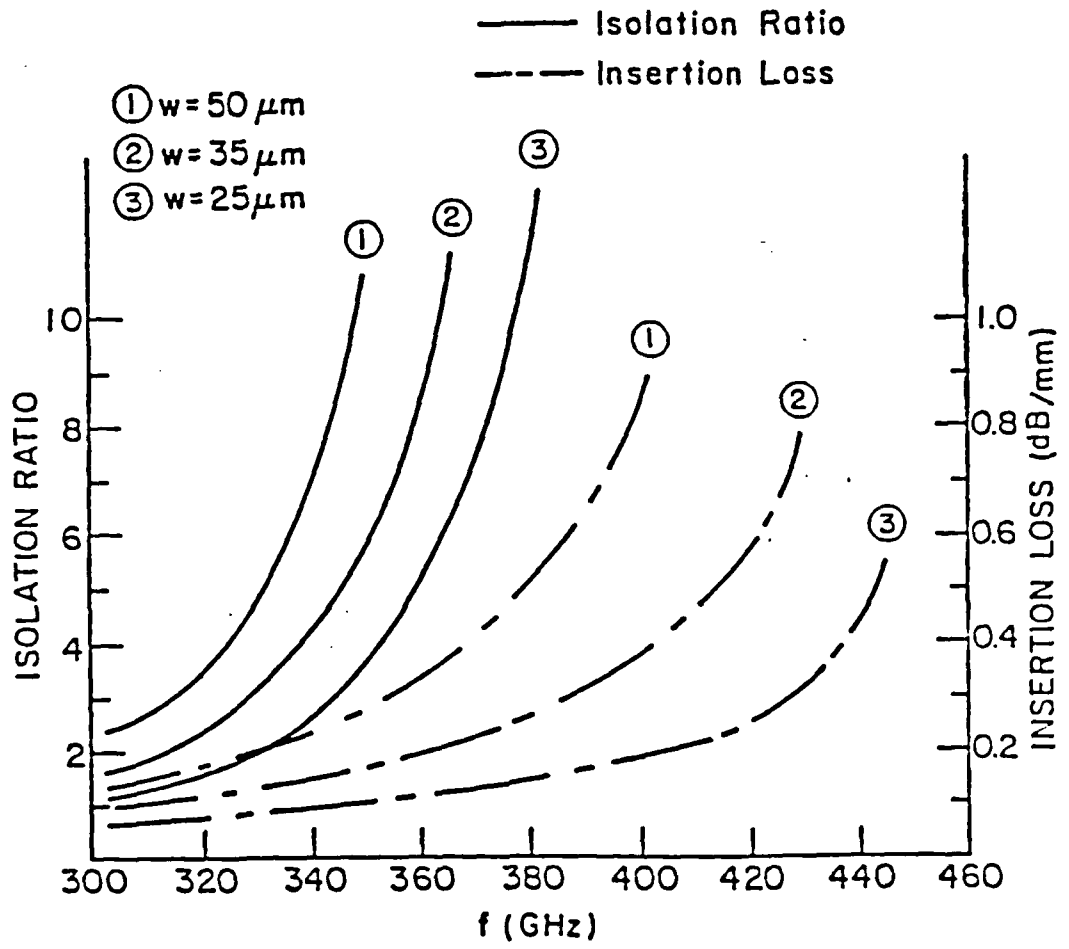

Figure 6a.
Isolation ratio and insertion loss as functions of frequency for three GaAs slab widths. The other parameters for the structure (Figure 1) are $\varepsilon_1 = 4$, $\varepsilon_3 = 1$ and T = 25μm.

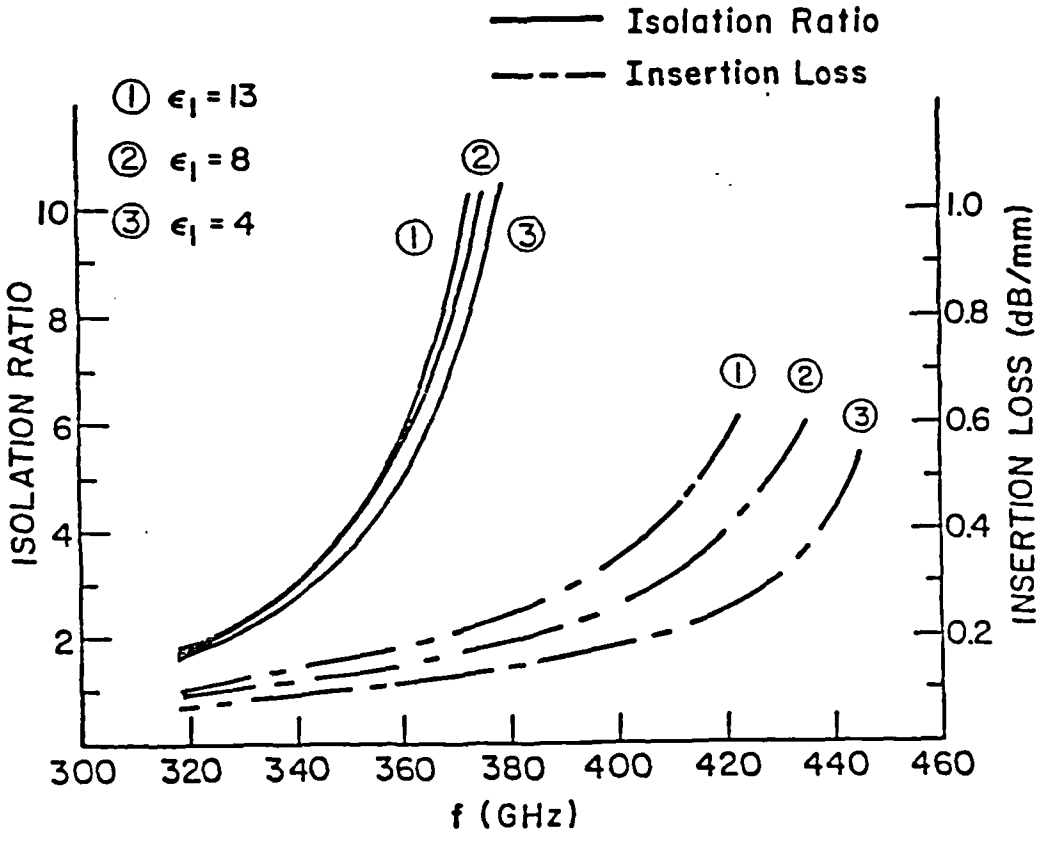

Figure 6b. Isolation ratio and insertion loss as functions of frequency for three ϵ_1 values. The other parameters are $\epsilon_3 = 1$, T = W = 25μm.

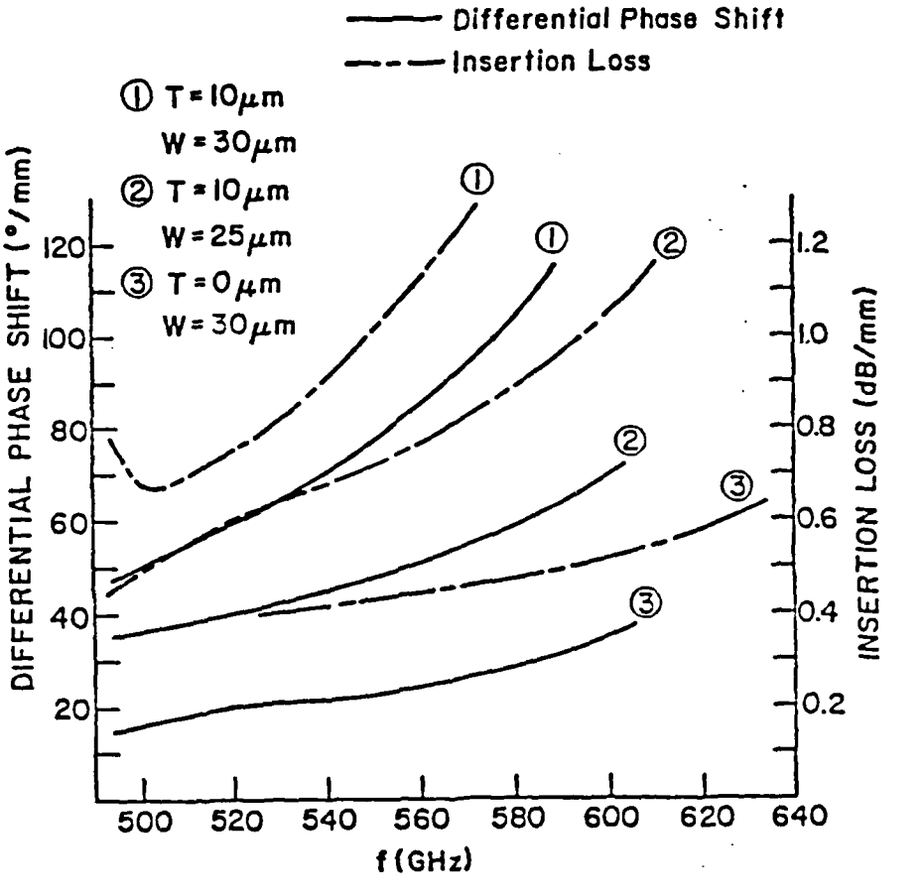

Figure 7. Differential phase shift and insertion loss as functions of frequency for three device configurations. Here, $\varepsilon_1 = 13$ and $\varepsilon_3 = 1$ (see Fig. 1).

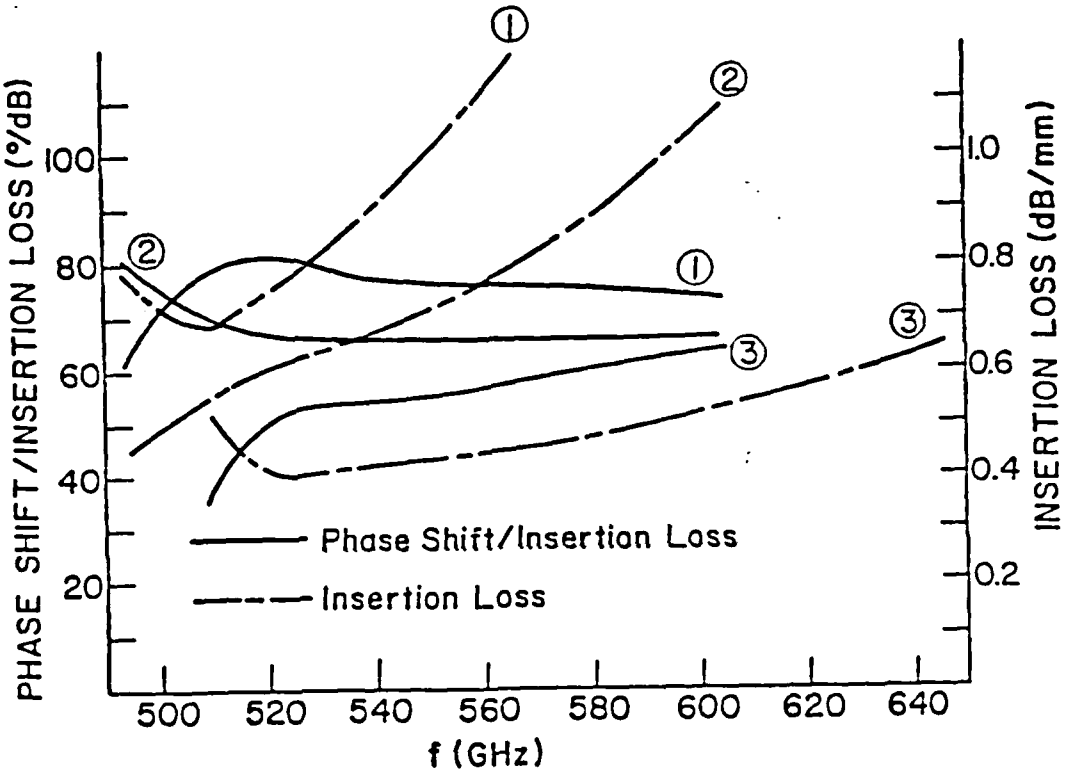

Figure 8. Differential phase shift-insertion loss ratio and insertion loss as functions of frequency for the same cases as in Figure 7.

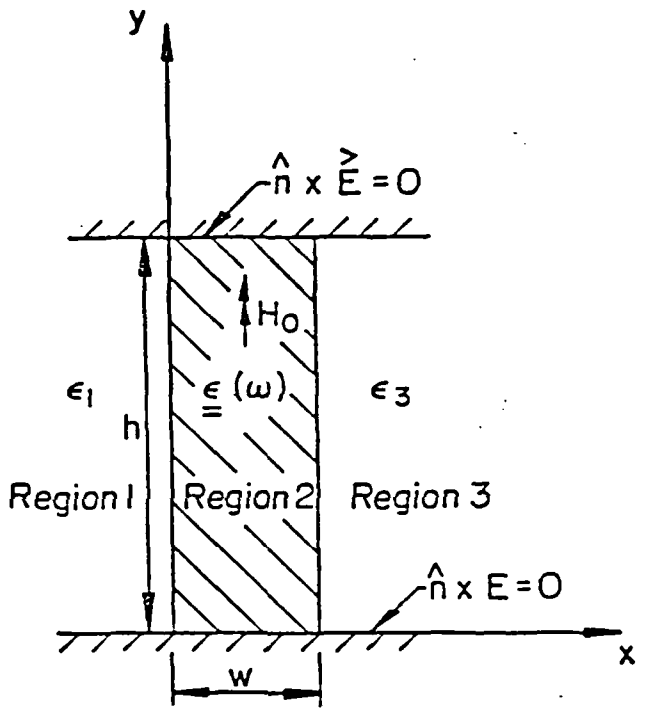

Figure 9. H-guide structure. Wave propagates along $\hat{z}$-direction.

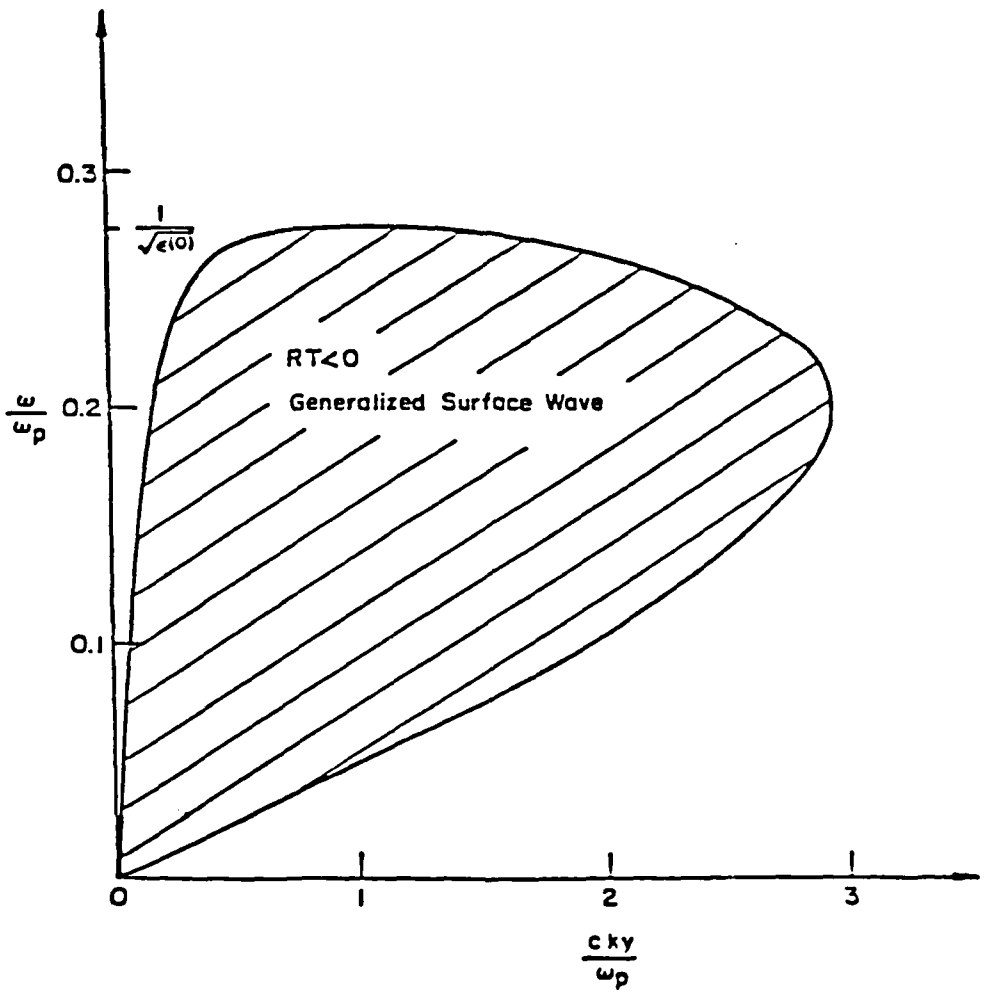

Figure 10.

Regions of 'true' and 'generalized' surface waves defined as functions of normalized frequency and wave number.

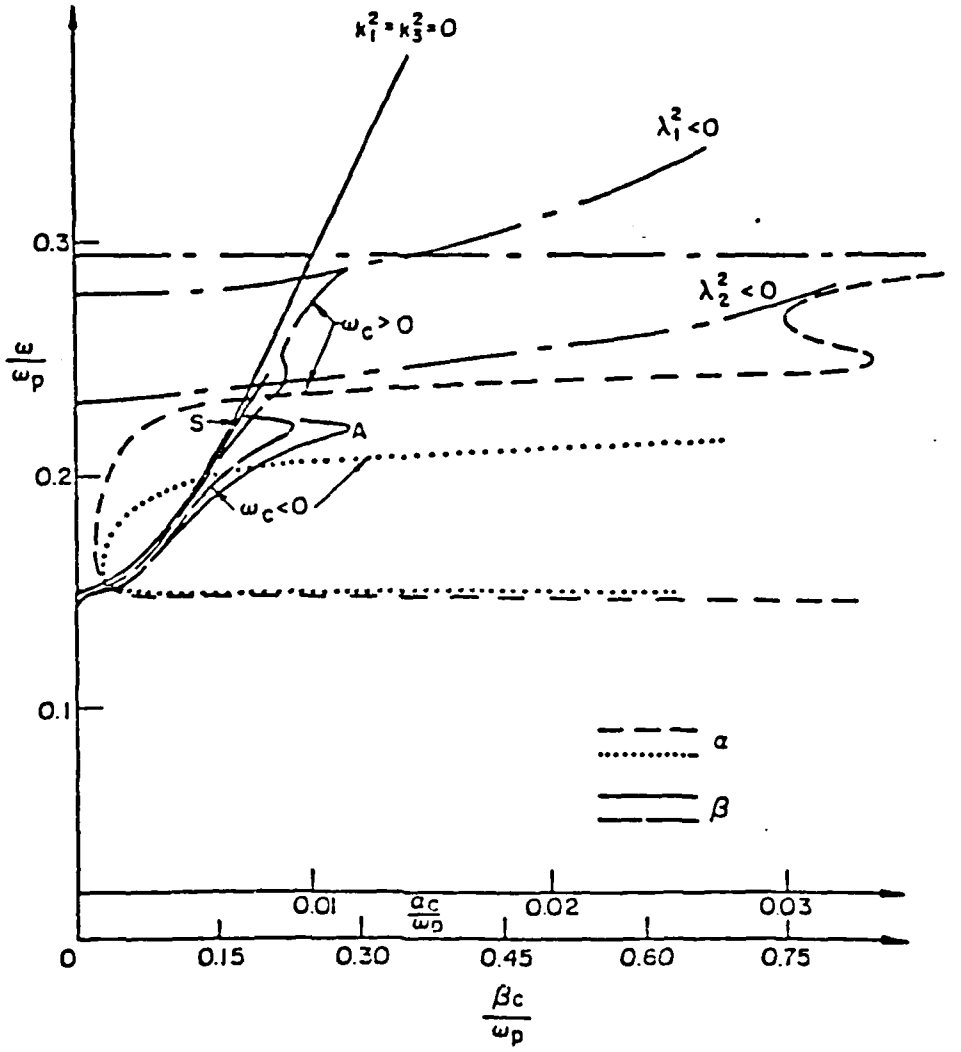

Figure 11a. Loss and dispersion curves of single interface structure (broken line system). Dispersion curve (S and A branches) of slab structure (solid line system). Here $\varepsilon_1 = \varepsilon_3 = 1$, $W = 0.4(2\pi c/\omega_p)$, $k_y c/\omega_p = 0.15$ and $\tau = 80/\omega_p$.

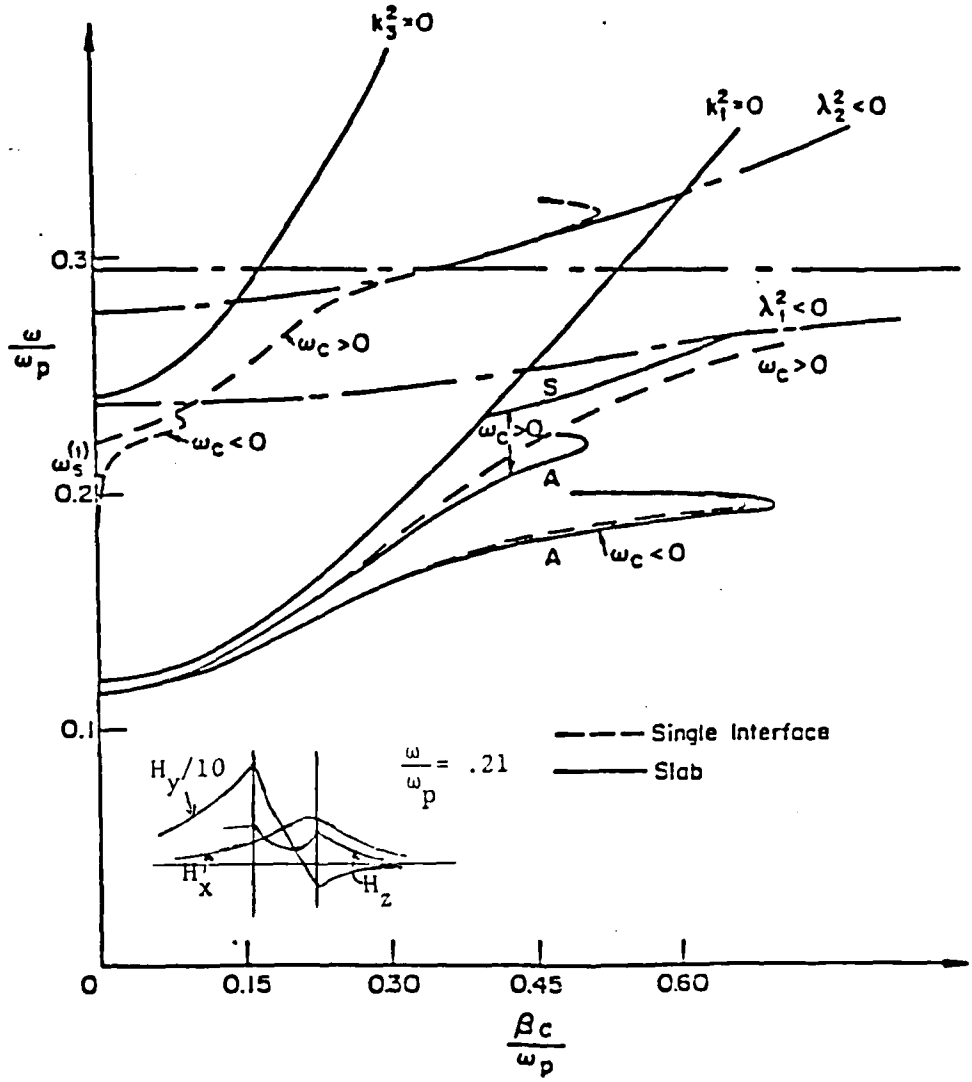

Figure 11b.
Dispersion curves of single interface and asymmetrically loaded slab structure with $\epsilon_1 = 4$, $\epsilon_3 = 1$, $W = 0.4(2\pi c/\omega_p)$ and $k_y c/\omega_p = 0.24$.

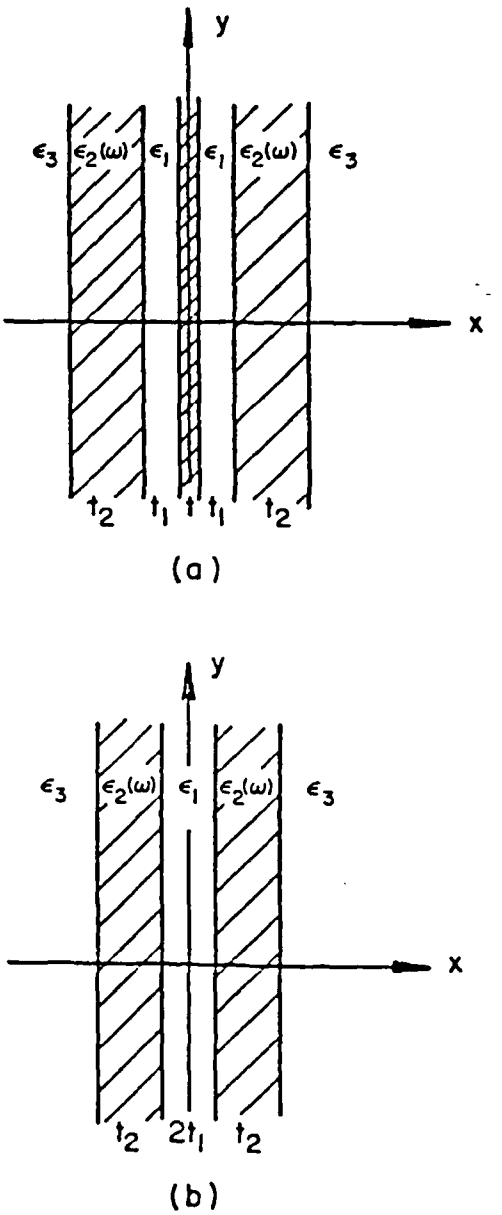

Figure 12. Planar structure used for difference frequency generation.

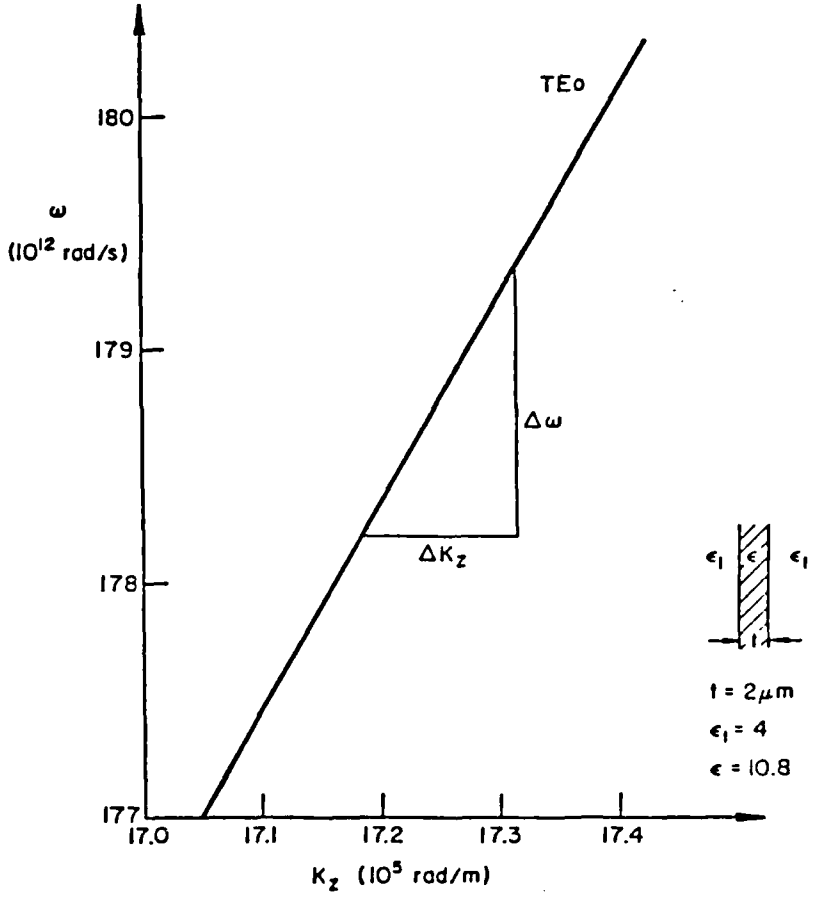

Figure 13. Dispersion diagram of the input optical waves.

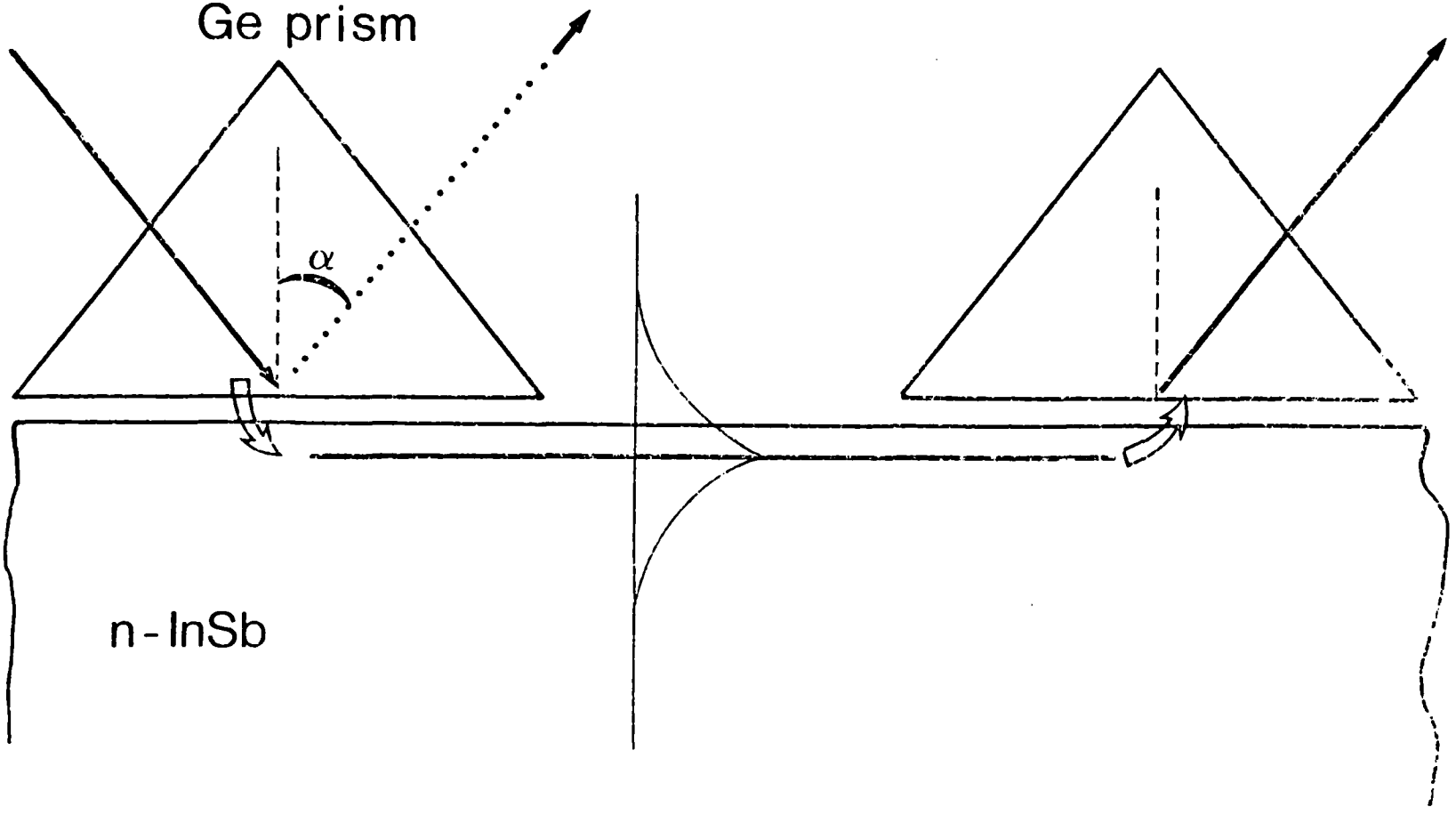

Figure 14. Schematic diagram for prism coupling to a single-interface structure.

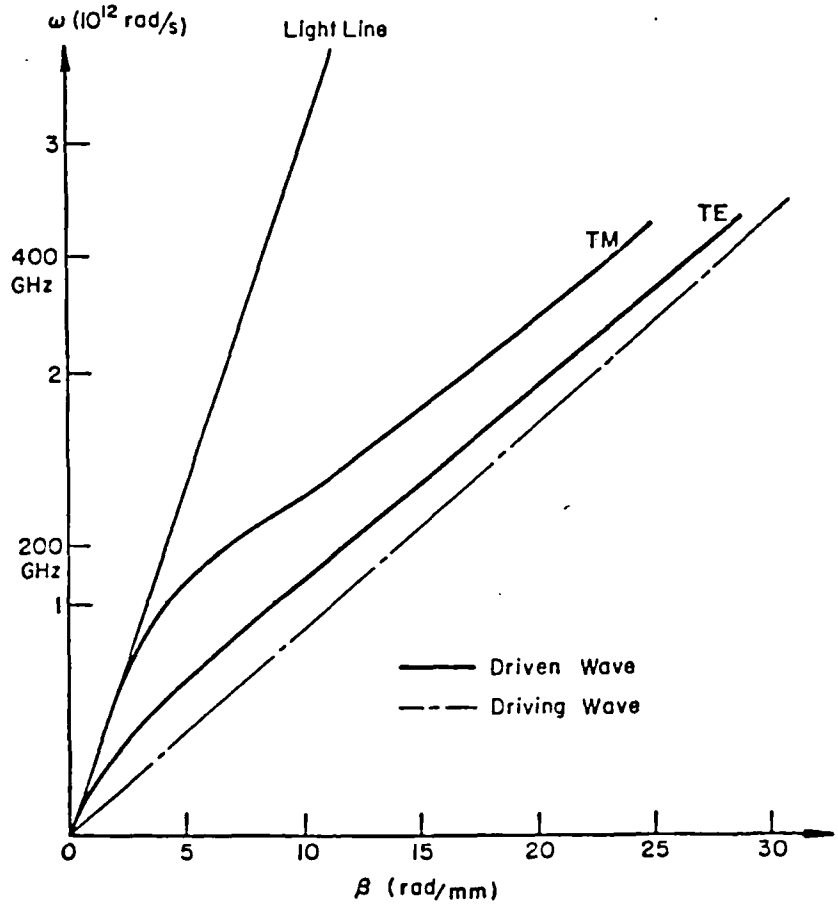

Figure 15. Dispersion curves of driving and driven waves in planar intrinsic GaAs structure.

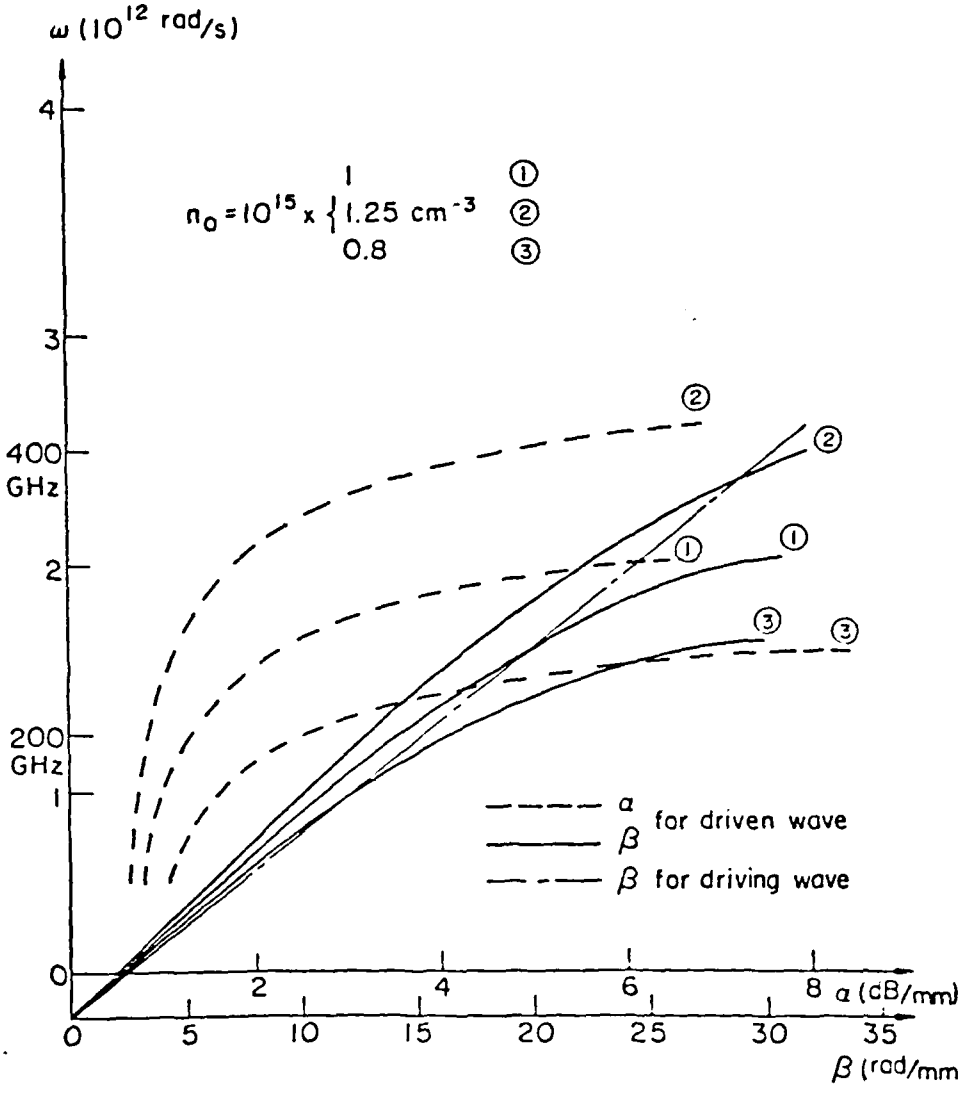

Figure 16. Phase-match condition for different plasma concentration.

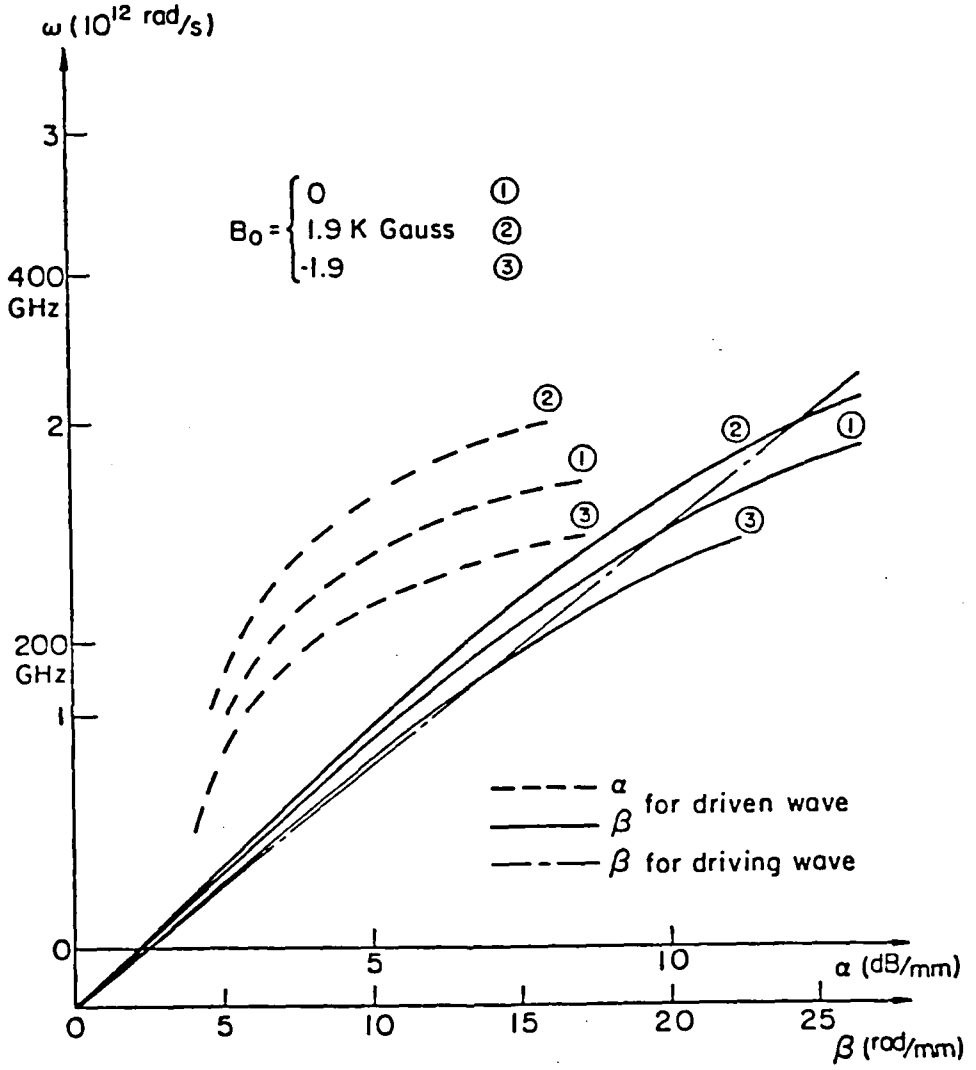

Figure 17. Phase-match condition for different d.c. magnetic field strengths.

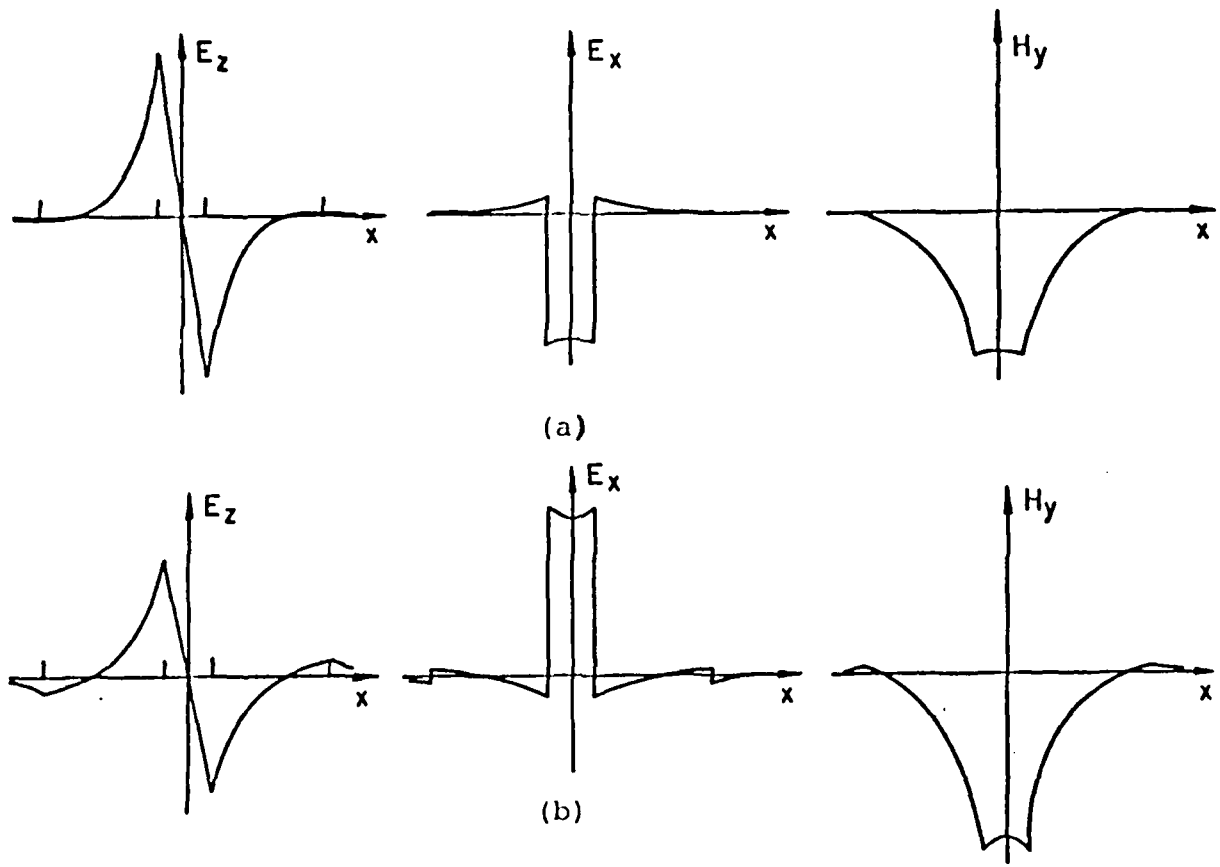

Figure 18. Field distribution of Even-TM modes.
(a) Forward direction of propagation.
(b) Reverse direction of propagation.

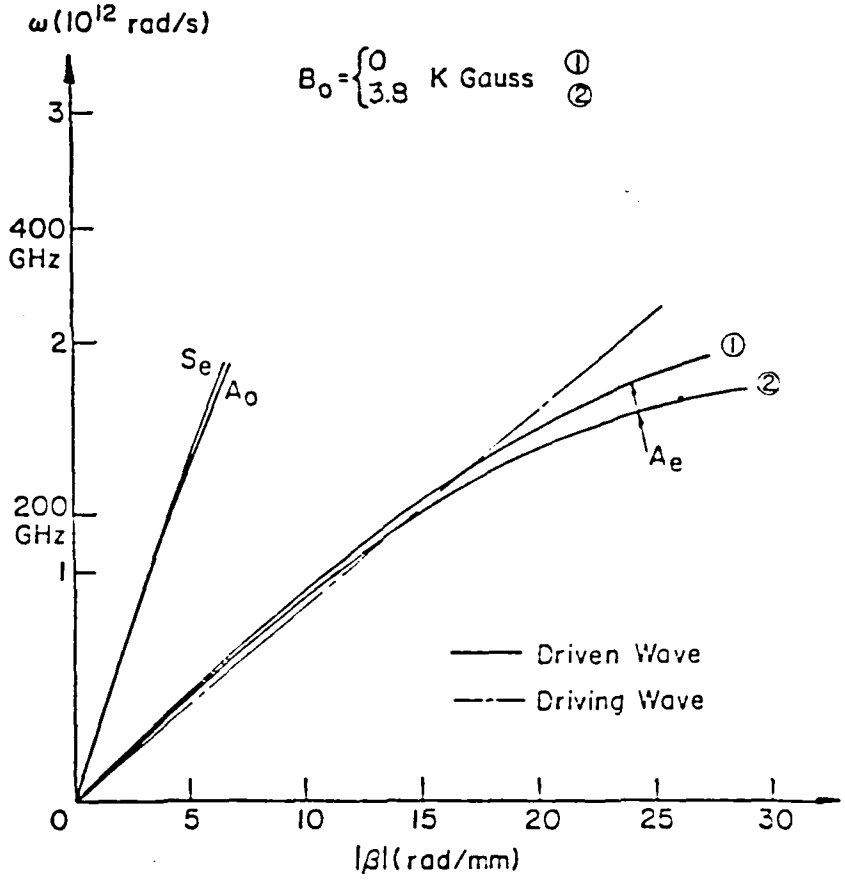

Figure 19. Dispersion diagram of MM waves in the presence of an uniform magnetic field.

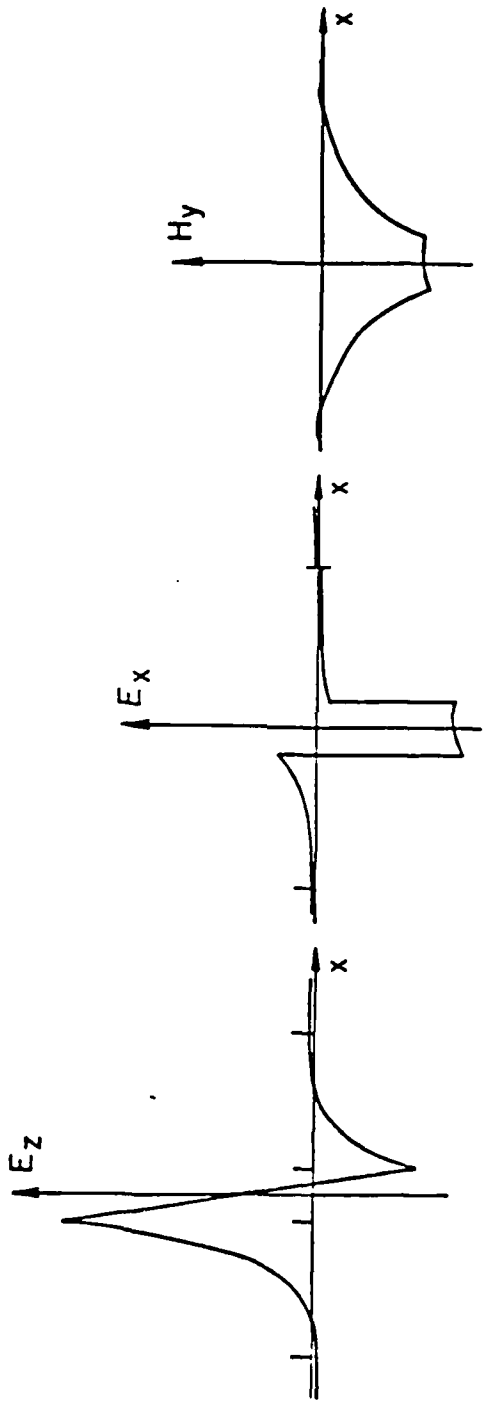

Figure 20. Field distribution of mode A_e.

III. References

1. M. F. Hoyaux, chapter 8 in Solid State Plasmas, Applied Physics Series, Vol. 2, Pion Limited, London, 1970

2. S. H. Talisa, "A Study of Surface Magnetoplasmon Based Near-Millimeter Wave Devices", Ph.D. dissertation, Brown University, 1982

3. A. V. Nurmikko, D. M. Bolle and S. H. Talisa, "Guiding and Control of Millimeter Waves by Surface Plasmon Phenomena in Semiconductors", Int. J. Infrered Millimeter Waves, 1, 1(1980)

4. R. F. Wallis, J. J. Brion, E. Burstein and A. Hartstein, "Theory of Surface Polaritons in Anisotropic Dielectric Media with Applications to Surface Magnetoplasmons in Semiconductors", phys. Rev., B9, 3424(1974)

5. B. G. Martin, A. A. Maradudin and R. F. Wallis, "Theory of Damped Surface Magnetoplasmons in n-Type InSb", Surface Sci., 77, 416(1978)

6. E. D. Palik, R. W. Gammon, H. Kaplan, R. F. Wallis and J. J. Quinn, "Coupled Surface Magnetoplasmons-Optic-phonon Polariton Modes on InSb", Phys. Rev., B13, 2497(1976)

7. J. J. Brion, R. F. Wallis, A. Hartstein, E. Burstein, "Interaction of Surface Magnetoplasmons and Surface Optical Phonons in Polar Semiconductors", Surface Sci., 34, 73(1973)

8. D. M. Bolle, S. H. Talisa, "Fundamental Considerations in Millimeter and Near-Millimeter Component Design Employing Magnetoplasmons", IEEE Trans. Microwave Theory Tech., MTT-29, 916(1981)

9. S. H. Talisa, D. M. Bolle, "Performance Predictions for Isolators and Differential Phase Shiftera for the Near-Millimeter Wave Range", Ibid, 1338(1981)

10. W. L. Hwang, S. H. Talisa, D. M. Bolle, "New Results for Near-MillimeterWave Isolators and Phase Shifters Based on Magnetoplasmons on GaAs Substrates", Int. J. Infrared Millimeter Waves, 3, 253(1982)

11. W. L. Hwang, D. M. Bolle, "Magnetoplasma Surface Wave Analysis for an H-guide Structure Containing Semiconductor", Ibid, 4, 819(1983)

12. G. S. Kovener, R. W. Alexander, R. J. Bell, "Surface Electromagnetic Waves with Damping. I. Isotropic Media", Phys. Rev., B14, 1458(1976)

13. for example, B. Lax and K. Button, p. 402 in Microwave Ferrites and Ferrimagnetics, McGraw-Hill, N. Y., 1962

14. T. Y. Chang, Opt. Commun., 2, 77(1970)

15. K. M. Baird, H. D. Riccius, K. J. Siemsen, "CO_2 Wavelengths and the Velocity of Light", Ibid. 6, 91(1972)

16. F Zernike and J. E. Midwinter, chapter 2 in Applied Nonlinear Optics, John Wiley and Sons, N. Y. 1973

17. Y. R. Shen, p. 28 in Nonlinear Infrared Generation, Topics in Applied Physics, vol. 16, Springer-Verlag, Berlin, Heidelberg, N.Y., 1977

18. D. H. Martin, K. Mizuno, "The Generation of Coherent Submillimeter Waves", Advances in Phys., v25, no3, 211(1976)

19. R. L. Aggarwal, B. Lax, H. R. Fetterman, P. E. Tannenwald, B. J. Clifton, "CW Generation of Tunable Narrow-Band Far-Infrared Radiation". J. Appl. Phys., 45, 3972(1974)

20. H. Cheng, P. B. Miller, "Nonlinear Optical Theory in Solids", Phys. Rev., 134, A683(1964)

21. J. Rudnick, E. A. Stern, "Second Harmonic Radiation from Metal Surfaces", Phys. Rev., B4, 4274(1971)

22. for ex., H.-G. Unger, chapter 2 in Planar Optical Waveguides and Fibres, Clarendon Press, Oxford, 1977

23. L. Bonsall, A. A. Maradudin, "Nonlinear Interaction of Surface Polaritons", J. Appl. Phys., 49(1), 253(1978)

24. A. A. Maradudin, D. L. Mills, "Scattering and Absorption of Electromagnetic Radiation by a Semi-infinite Medium in the Presence of Surface Roughness", Phys. Rev., B11, 1392(1975)

25. R. E. Collin, chapter 11 in Field Theory of Guided Waves, McGraw-Hill, N.Y., 1961

26. N. Van Tran, C. K. Patel, "Free-Carrier Magneto-Optical Effects in Far-Infrared Difference-Frequency Generation in Semiconductors", Phys. Rev. Lett., 22, 463(1969)

27. A. M. Vaucher, C. D. Striffler, C. H. Lee, "Theory of Optically Controlled Millimeter Wave Phase Shifters", IEEE Trans. Microwave Theory Tech., MTT-31, 209(1983)

28. K. E. Mortenson, A. L. Armstrong, J. M. Borrego, J. F. White, "A Review of Bulk Semiconductor Microwave Control Components", IEEE Proc., 59(8), 1191(1971)

29. R. F. Whitmer, E. B. Barrett, "Nonlinear Interaction of an Electromagnetic Wave with a Plasma Layer in the Presence of a Static Magnetic Field. II. Higher Harmonic and a Nonlinear Propagation Theory", Phys. Rev., 121, 661(1961)

30. B. Lax, W. Zawadxki, M. H. Weiler, "Nonlinear Magneto-Optics of Electrons and Holes in Semiconductors and Semimetals", Phys. Rev. Lett., 18, 462(1967)

31. M. Kobayashi, "Reciprocity Theorem for a Region with Inhomogeneous Bianisotropic Media and Surface Impedance", IEEE Trans. Microwave Theory Tech., MTT-24, 114(1976)

32. H. L. Stormer, A. G. Gossard, W. Wiegmann, K. Baldwin, Appl. Phys. Lett., 39, 912 (1981).

33. G. H. Dohler et al., Phys. Rev. Lett., 47, 864 (1981).

END

FILMED

9-84

DTIC